Physics at the large hadron collider

N. V. Krasnikov and V. A. Matveev
Institute of Nuclear Research, Russian Academy of Sciences, Moscow 117312

Fiz. Élem. Chastits At. Yadra **28**, 1125–1189 (September–October 1997)

The physics to be investigated at the large hadron collider (LHC) is reviewed. The main parameters of the CMS and ATLAS detectors are described. © *1997 American Institute of Physics.* [S1063-7796(97)00305-7]

1. INTRODUCTION

The scientific program at the large hadron collider (LHC),[1,2] which will be the largest particle-accelerator complex ever built in the world, has many goals. Among them there are two supergoals:

(a) Discovery of the Higgs boson in the standard electroweak Weinberg–Salam model.

(b) Discovery of supersymmetry.

LHC will accelerate two proton beams with total energy $\sqrt{s}=14$ TeV. At the low-luminosity stage (the first two to three years of operation) the luminosity is planned to be $L_{\text{low}}=10^{33}\ \text{cm}^{-2}\text{s}^{-1}$ with total luminosity $L_{\text{tot}}=10^{4}\ \text{pb}^{-1}$ per year. At the high-luminosity stage the luminosity is planned to be $L_{\text{high}}=10^{34}\ \text{cm}^{-2}\text{s}^{-1}$ with total luminosity $L_{\text{tot}}=10^{5}\ \text{pb}^{-1}$ per year. The LHC will start operation in the year 2005. There are many lines of research for LHC:

(a) Discovery of the Higgs boson in the standard electroweak Weinberg–Salam model.

(b) Discovery of supersymmetry.

(c) B physics.

(d) Heavy-ion physics.

(e) Top-quark physics.

(f) Standard physics (QCD, electroweak interactions).

(g) The search for new physics beyond the minimal supersymmetric model and the Weinberg–Salam model.

There are planned to be two large detectors at LHC—CMS (Compact Muon Solenoid) and ATLAS.

In this paper we describe the main parameters of the CMS and ATLAS detectors and review the main physics to be investigated at LHC.[1)]

2. DETECTORS

2.1. CMS detector

Subdetectors. The CMS detector consists of the following subdetectors:

(1) Tracker barrel detector (TB).
(2) Tracker forward detector (TF).
(3) ECAL (electromagnetic calorimeter) barrel detector (EB).
(4) ECAL forward (endcap) detector (EF).
(5) Preshower in front of barrel ECAL (SB).
(6) Preshower in front of forward ECAL (SF).
(7) HCAL (hadronic calorimeter) barrel detector (HB).
(8) HCAL forward (endcap) detector (HF).
(9) Very forward calorimeter (VF).
(10) Barrel muon station (MS).
(11) Forward muon station (MF).

Basic goals and design considerations. One of the most important tasks for LHC is the quest for the origin of the spontaneous symmetry-breaking mechanism in the electroweak sector of the standard model (SM). Namely, all the renormalizable models of electroweak interactions are based on the use of gauge symmetry breaking. As a consequence of the electroweak symmetry breaking and the renormalizability of the theory, there must be a neutral scalar particle (Higgs boson) in the spectrum. The existing LEP1 bound on the Higgs-boson mass in the SM is $m_h \geq 64$ GeV. LEP2 with the full energy $\sqrt{s}=190$–195 GeV will be able to reveal the Higgs boson in the SM with a mass of up to $m_h \leq 90$–95 GeV. The theoretical bound based on tree-level unitarity gives the upper bound $m_h \leq 1$ TeV for the Higgs-boson mass. A similar bound $m_h \leq 700$–800 GeV is given by lattice-based estimates. In the minimal supersymmetric extension of the SM (MSSM) the lightest Higgs boson must be relatively light: $m_h \leq 120$ GeV. Other nonminimal supersymmetric models of electroweak interactions typically predict a relatively small mass for the lightest Higgs boson: $m_h \leq 160$–180 GeV. Thus, the discovery of the Higgs boson would be a check of spontaneous symmetry breaking and of the renormalizability of the theory, and there is no doubt that it is the supergoal number 1 for LHC. The Higgs search is therefore used as a first benchmark for detector optimization for both CMS and ATLAS. For the SM Higgs boson, the detector has to be sensitive to the following processes in order to cover the full mass range above the expected LEP2 discovery limit of 90–95 GeV:

(A) $h \to \gamma\gamma$ mass range 90 GeV $\leq m_h \leq$ 150 GeV.

(B) $h \to b\bar{b}$ from Wh, Zh, $t\bar{t}h$ using an $^{\pm}$ ($l^{\pm}=e^{\pm},\mu^{\pm}$) tag and b tagging in the mass range 80 GeV $\leq m_h \leq 100$ GeV.

(C) $h \to ZZ^* \to 4l^{\pm}$ for the mass range 130 GeV $\leq m_h \leq 2m_Z$.

(D) $h \to ZZ \to 4l^{\pm}$, $2l^{\pm}2\nu$ for the mass range $m_h \geq 2m_Z$.

(E) $h \to WW$, $ZZ \to l^{\pm}\nu$ (2 jets), $2l^{\pm}$ (2 jets), using tagging of forward jets for m_h up to 1 TeV.

In the minimal supersymmetric extension of the standard model (MSSM) there is a family of Higgs particles ($H^{\pm},h,H,A$). Thus, in addition to the standard Higgs-boson signatures the MSSM Higgs searches are based on the following processes:

(F) $A \to \tau^+\tau^- \to e\mu$ plus ν's, or $A \to \tau^+\tau^- \to l^{\pm}$ plus hadrons plus ν's.

(G) $H^{\pm} \to \tau^{\pm} \nu$ from $t\bar{t} \to H^{\pm} W^{\mp} b\bar{b}$ and $H^{\pm} \to 2$ jets, using an $l^{\pm}$ tag and b tagging.

The observable cross sections for most of these processes are small (1–100 pb) over a large part of the mass range. Thus, it is necessary to work at high luminosity and to maximize the detectable rates above the backgrounds by high-resolution measurements of electrons, muons, and photons.

For the $H^{\pm}$ and A signatures in the case of the MSSM, high-performance detector capabilities are also required for the measurements, which are expected to be best achieved at initial luminosities with a low level of overlapping events, namely, secondary vertex detection for τ leptons and b quarks, and high-resolution calorimetry for jets and missing transverse energy E_T^{miss}.

The second supergoal of the LHC project is the discovery of supersymmetry, i.e., the detection of superparticles. Here the main signature is events with missing transverse energy, which are a consequence of the undetected lightest stable supersymmetric particles (LSP) predicted in supersymmetric models with R-parity conservation. Therefore, it is necessary to set stringent requirements for the hermeticity and E_T^{miss} capability of the detector. In addition, the search for new physics different from supersymmetry (new gauge bosons W' and Z', new Higgs bosons with large Yukawa couplings, etc.) at LHC requires high-resolution lepton measurements and charge identification even in the p_T range of a few TeV. Other possible signatures of new physics (compositeness) can be provided by very high-p_T jet measurements. An important task of LHC is the study of B and T physics. Even at low luminosities the LHC will be a high-rate beauty- and top-quark factory. The main emphasis in B physics is the precise measurement of CP violation in the B_d^0 system and the determination of the Kobayashi–Maskawa angles. In addition, investigations of $B\bar{B}$ mixing in the B_S^0 system and rare B decays are also very important. Precise secondary-vertex determination, full reconstruction of final states with relatively low-p_T particles (an example is $B_d^0 \to J/\Psi K_S^0$ followed by $J/\Psi \to l^+ l^-$ and $K_S^0 \to \pi^+ \pi^-$), and low-p_T lepton first-level triggering capability are all necessary. Besides running as a proton–proton collider, LHC will be used to collide heavy ions at a center-of-mass energy 5.5 TeV per nucleon pair. The formation of quark–gluon plasma in heavy-ion collisions is predicted to be signaled by a strong suppression of Υ' and Υ'' production relative to Υ production when compared with pp collisions. The CMS and ATLAS detectors will be used to detect low-momentum muons produced in heavy-ion collisions and to reconstruct Υ, Υ', and Υ'' production. Therefore, the basic design considerations for both ATLAS and CMS are the following:

1. Very good electromagnetic calorimetry for electron and photon identification and measurements.

2. Good hermetic jet and missing-E_T calorimetry.

3. Efficient tracking at high luminosity for lepton-momentum measurements, for b-quark tagging, and for enhanced electron and photon identification, as well as tau and heavy-flavor vertexing and reconstruction capability of some B decay final states at lower luminosity.

4. Stand-alone, precision muon-momentum measurement up to the highest luminosity, and very low-p_T trigger capability at lower luminosity.

5. Large acceptance in η coverage.

Brief description of CMS subdetectors

Tracker. The design goal of the cental tracking system is to reconstruct isolated high-p_T tracks with an efficiency better than 95% and high-p_T tracks within jets with an efficiency of better than 90% in the rapidity range $|\eta| \leqslant 2.6$. The momentum resolution required for isolated charged leptons in the central rapidity region is $\delta p_T / p_T = 0.1 p_T$ (p_T in TeV). This will allow the measurement of the lepton charge up to $p_T = 2$ TeV. It is also very important for the tracking system to perform efficient b and τ tagging. The tracker system consists of silicon pixels, and silicon and gas microstrip detectors (MSGS), which provide precision momentum measurements and ensure an efficient pattern of recognition even at the highest luminosity. A silicon pixel detector consists of two barrel layers and three endcap layers, and it is placed close to the beam pipe with the tasks of:

(a) assisting in pattern recognition by providing two or three true space points per track over the full rapidity range in the main tracker;

(b) improving the impact-parameter resolution for b tagging;

(c) allowing 3-dimensional vertex reconstruction by providing a much improved Z resolution in the barrel part.

The silicon microstrip detector is required to have a powerful vertex-finding capability in the transverse plane in a large momentum range for b tagging and heavy-quark physics, and it must be able to distinguish different interaction vertices at high luminosity. The CMS silicon microstrip detector is subdivided into barrel and forward parts, meeting at $|\eta| = 1.8$ [$\eta \equiv -\ln(\tan(\theta/2))$], providing at least three measuring points on each track for $|\eta| \leqslant 2.6$. The microstrip gas chambers provide a minimum of seven hits for high-p_T tracks. The track-finding efficiency in the tracker is 98% for $p_T \geqslant 5$ GeV. The charged-particle momentum resolution depends on the values of η and p_T of the charged particle, and for $p_T = 100$ GeV and $|\eta| \leqslant 1.75$ it is above 2%. The impact-parameter resolution also depends on p_T and η, and for 10 GeV $\leqslant p_T \leqslant$ 100 GeV and $|\eta \leqslant 1.3$ in the transverse plane it is about 100 μm. The b-tagging efficiency from $t\bar{t}$ decays should be better than 30%. A significant impact parameter can be used to tag τ leptons. It could be useful in searches such as SUSY Higgs-boson decays A, H, $h \to \tau\tau \to e + \mu + X$ (or l+hadrons). These leptons (hadrons) originate from secondary (τ) vertices, while in the backgrounds from $t\bar{t} \to Wb + W\bar{b} \to e + \mu + X$ and $WW \to e + \mu + X$ they originate from the primary vertex. It is possible to have an efficiency for the signal of $\approx 50\%$, while for the background channels it is $\approx 3\%$.

ECAL. The barrel part of the electromagnetic calorimeter covers the rapidity interval $|\eta| \leqslant 1.56$. The endcaps cover the interval $1.65 \leqslant |\eta| \leqslant 2.61$. The gaps between the barrel and the endcaps are used to route the services of the tracker and preshower detectors. The barrel granularity is

432-fold in ϕ and 108×2-fold in η. A very good intrinsic energy resolution given by

$$\frac{\sigma}{E}=\frac{0.02}{\sqrt{E}}\oplus0.005\oplus\frac{0.2}{E} \tag{1}$$

is assumed for electrons and photons with a $PbWO_4$ crystal ECAL. The physics process that imposes the strictest performance requirements on the electromagnetic calorimeter is the intermediate-mass Higgs decaying into two photons. The main goal here is to obtain very good diphoton mass resolution. The mass resolution has terms that depend on the resolution in energy (E_1,E_2) and on the two-photon angular separation (θ), and it is given by

$$\frac{\sigma_M}{M}=\frac{1}{2}\left[\frac{\sigma_{E_1}}{E_1}\oplus\frac{\sigma_{E_2}}{E_2}\oplus\frac{\sigma_\theta}{\left(\tan\left(\frac{\theta}{2}\right)\right)}\right], \tag{2}$$

where $\oplus$ denotes a quadratic sum, E is in GeV, and θ is in radians. For the Higgs two-photon decay at LHC the angular term in the mass resolution can become important, so that it is necessary to measure the direction of the photons using the information from the calorimeter alone. In the barrel region $|\eta|\leq1.56$ the angular resolution is supposed to be $\sigma_\theta \leq 50$ mrad/$\sqrt{E}$. Estimates give the following diphoton mass resolution for the $h\rightarrow\gamma\gamma$ channel ($m_h=100$ GeV):

$\delta m_{\gamma\gamma}=475$ MeV (low luminosity L $=10^{33}$ cm^{-2}s^{-1}),

$\delta m_{\gamma\gamma}=775$ MeV (high luminosity L $=10^{34}$ cm^{-2}s^{-1}).

HCAL. The hadron calorimeter surrounds the electromagnetic calorimeter and acts in conjunction with it to measure the energies and directions of particle jets, and to provide hermetic coverage for measurement of the transverse energy. The pseudorapidity range ($|\eta|\leq3$) is covered by the barrel and endcap hadron calorimeters which sit inside the $4T$ field of the CMS solenoid. In the central region around $\eta=0$ a hadron shower "tail catcher" is installed outside the solenoid coil to ensure adequate sampling depth. The active elements of the barrel and endcap hadron calorimeter consist of plastic scintillator tiles with wavelength-shifting fiber readout. The pseudorapidity range ($3.0\leq\eta\leq5.0$) is covered by a separate very forward calorimeter. The hadron calorimeter must have good hermeticity, good transverse granularity, moderate energy resolution, and sufficient depth for hadron-shower containment. The physics program requires good hadron resolution and segmentation to detect narrow states decaying into pairs of jets. The dijet mass resolution includes contributions from physics effects such as fragmentation as well as detector effects such as angular and energy resolution. The energy resolution is assumed to be

$$\frac{\Delta E}{E}=\frac{0.6}{\sqrt{E}}\oplus0.03 \tag{3}$$

for $|\eta|\leq1.5$ and segmentation $\Delta\eta\times\Delta\Phi=0.1\times0.1$.

The dijet mass resolution is approximately the following:

1. 10–15% for 50 GeV$\leq p_T\leq$60 GeV and $m_{ij}=m_Z$.
2. 5–10% for 500 GeV$\leq p_T\leq$600 GeV and $m_{ij}=m_Z$.

The expected energy resolution for jets in the very forward calorimeter is parametrized as

$$\frac{\sigma_{E_{\text{jet}}}}{E_{\text{jet}}}=\frac{1.28\pm0.01}{\sqrt{E_{\text{jet}}}}\oplus(0.02\pm0.01). \tag{4}$$

The expected missing-transverse-energy resolution in the CMS detector with very forward $2.5\leq\eta\leq4.7$ coverage is

$$\frac{\sigma_i}{\Sigma E_t}=\frac{0.55}{\sqrt{\Sigma E_t}} \tag{5}$$

(E_t in GeV). In the absence of the very forward calorimeter, the missing-transverse-energy resolution would be worse by nearly a factor of 3.

Muon system. At the LHC the effective detection of muons from Higgs bosons, W, Z, and $t\bar{t}$ decays requires coverage over a large rapidity interval. Muons from pp collisions are expected to provide clean signatures for a wide range of new physics processes. Many of these processes are expected to be rare and will require the highest luminosity. The goal of the muon detector is to identify these muons and to provide a precision measurement of their momenta from a few GeV to a few TeV. The barrel detector covers the region $|\eta|\leq1.3$. The endcap detector covers the region $1.3\leq|\eta|\leq2.4$. The muon detector must perform three basic tasks: muon identification, and trigger and momentum measurement. The muon detector is placed behind ECAL and the coil. It consists of four muon stations interleaved with the iron return yoke plates. The magnetic flux in the iron provides the possibility of an independent momentum measurement. The barrel muon detector is based on a system of 240 chambers of drift tubes arranged in four concentric stations. In the endcap regions, the muon detector comprises four muon stations. The muon detector has the following functionality and performance:

1. Geometric coverage: pseudorapidity coverage up to $|\eta|=2.4$ with the minimum possible acceptance losses due to gaps and dead areas.
2. Transverse-momentum resolution for the muon detector alone for $0\leq|\eta|\leq2$: $\Delta p_T/p_T=0.06$–0.1 for $p_T=10$ GeV, 0.07–0.2 for $p_T=100$ GeV, and 0.15–0.35 for $p_T=1$ TeV.
3. Transverse-momentum resolution after matching with the central detector for $0\leq|\eta|\leq2$: $\Delta p_T/p_T=0.005$–0.01 for $p_T=10$ GeV, 0.015–0.05 for $p_T=100$ GeV, and 0.05–0.2 for $p_T=1$ TeV.
4. Charge assignment: correct at 99% confidence level up to $p_T=7$ TeV for the full η coverage.
5. Muon trigger: precise muon chambers and fast dedicated detectors provide a trigger with p_T thresholds from a few GeV up to 100 GeV.

A schematic view of the CMS detector is shown in Figs. 1–3.

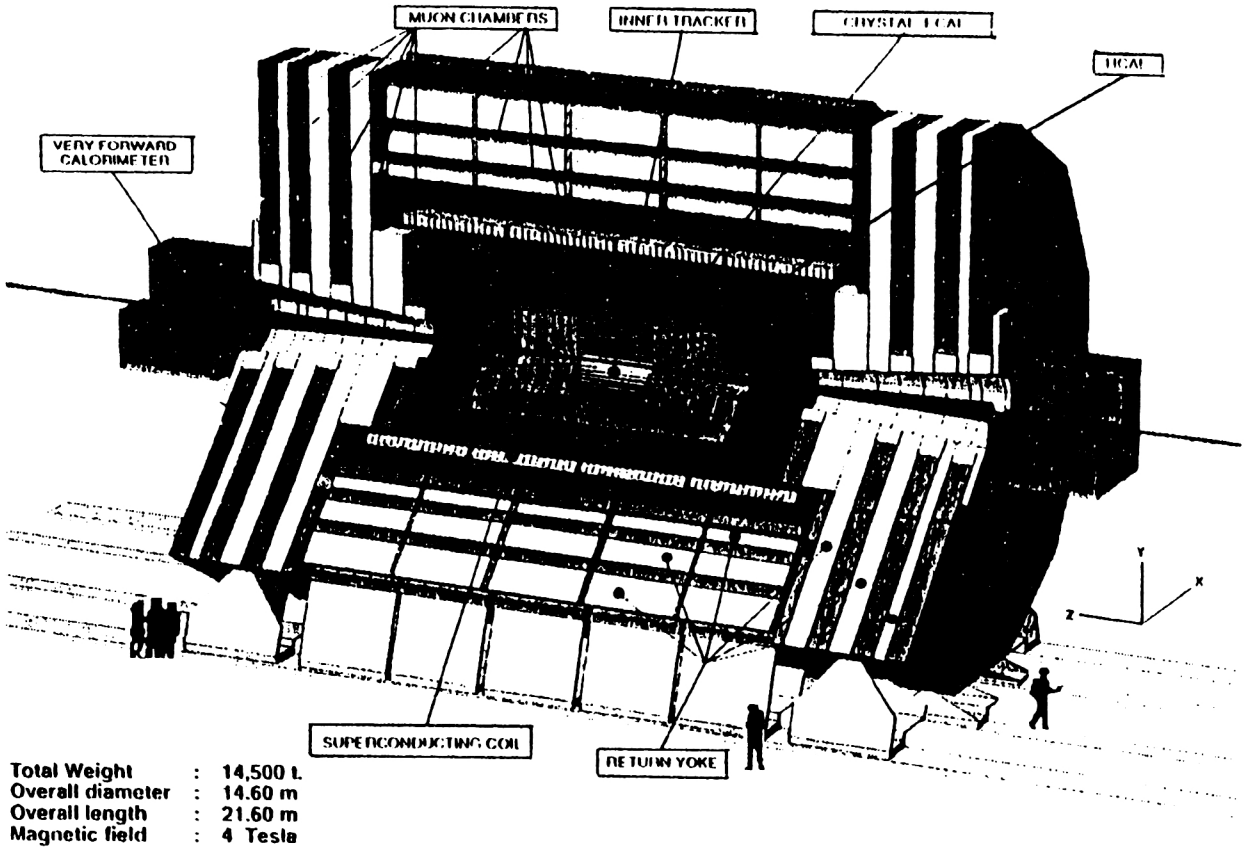

FIG. 1. Three-dimensional view of the CMS detector.

2.2. ATLAS detector

The design of the ATLAS detector is similar to that of the CMS detector. It also consists of an inner detector (tracker), an electromagnetic calorimeter, a hadron calorimeter, and a muon spectrometer. Here we briefly describe the main parameters of the ATLAS subdetectors.

Inner detector. The main parameters of the ATLAS inner detector are:

1. Tracking coverage over the pseudorapidity range $|\eta| \leqslant 2.5$.

2. Momentum resolution $\Delta p_T/p_T \leqslant 0.3$ at $p_T = 500$ GeV for $|\eta| \leqslant 2$, and no worse than 50% for $|\eta| = 2.5$.

3. Polar-angle resolution $\leqslant 2$ mrad.

4. Tracking efficiency $\geqslant 95\%$ over the full coverage for isolated tracks with $p_T \geqslant 5$ GeV, with fake-track rates less than 1% of signal rates.

5. Tagging of b jets with an efficiency $\geqslant 30\%$ at the highest luminosity, with a rejection $\geqslant 10$ against non-b hadronic jets.

6. For initial lower-luminosity running, the ability to reconstruct secondary vertices from b and τ decays and charged tracks from primary vertices and from secondary decay vertices of short-lived particles with $\geqslant 95\%$ efficiency for $p_T \geqslant 0.5$ GeV over the full coverage.

ECAL. The energy resolution is $\Delta E/E = 0.1/\sqrt{E} \oplus 0.007$ for $|\eta| \leqslant 2.5$. The diphoton mass resolution is estimated to be 1.4 GeV for a Higgs boson mass $m_h = 100$ GeV for $L = 10^{34}$ cm^{-2}s^{-1} (for CMS the diphoton mass resolution is 775 MeV).

HCAL. The jet energy resolution is $\Delta E/E = 0.5/\sqrt{E} \oplus 0.03$ for jets and a segmentation of $\Delta\eta \times \Delta\Phi = 0.1 \times 0.1$ for $|\eta| \leqslant 3$, and $\Delta E/\sqrt{E} = 1/\sqrt{E} \oplus 0.1$ and a segmentation of $\Delta\eta \times \Delta\Phi = 0.1 \times 0.1$ for a very forward calorimeter $3 \leqslant |\eta| \leqslant 5$.

Muon spectrometer. The muon momentum resolution is $\Delta p_T/p_T = 0.02$ ($p_T = 20$ GeV), $\Delta p_T/p_T = 0.02$ ($p_T = 100$ GeV), and $\Delta p_T/p_T = 0.08$ ($p_T = 1$ TeV) for $|\eta| \leqslant 3$.

3. PHYSICS AT LHC

3.1. Parton model

A high-energy proton beam can be regarded as an unseparated beam of quarks, antiquarks, and gluons. For the hard-scattering phenomena that are of principal interest for LHC the cross section for the hadronic reaction

$$a + b \to c + \text{anything} \tag{6}$$

is given in the parton model by the formula[3,4]

$$d\sigma(a+b\to c+X) = \sum_{\text{partons } i,j} f_i^{(a)} f_j^{(b)} d\hat{\sigma}(i+j\to c+X'), \tag{7}$$

where $f_i^{(a)}$ is the probability of finding constituent i in hadron a, and $\hat{\sigma}(i+j\to c+X')$ is the cross section for the elementary process leading to the desired final state. This pic-

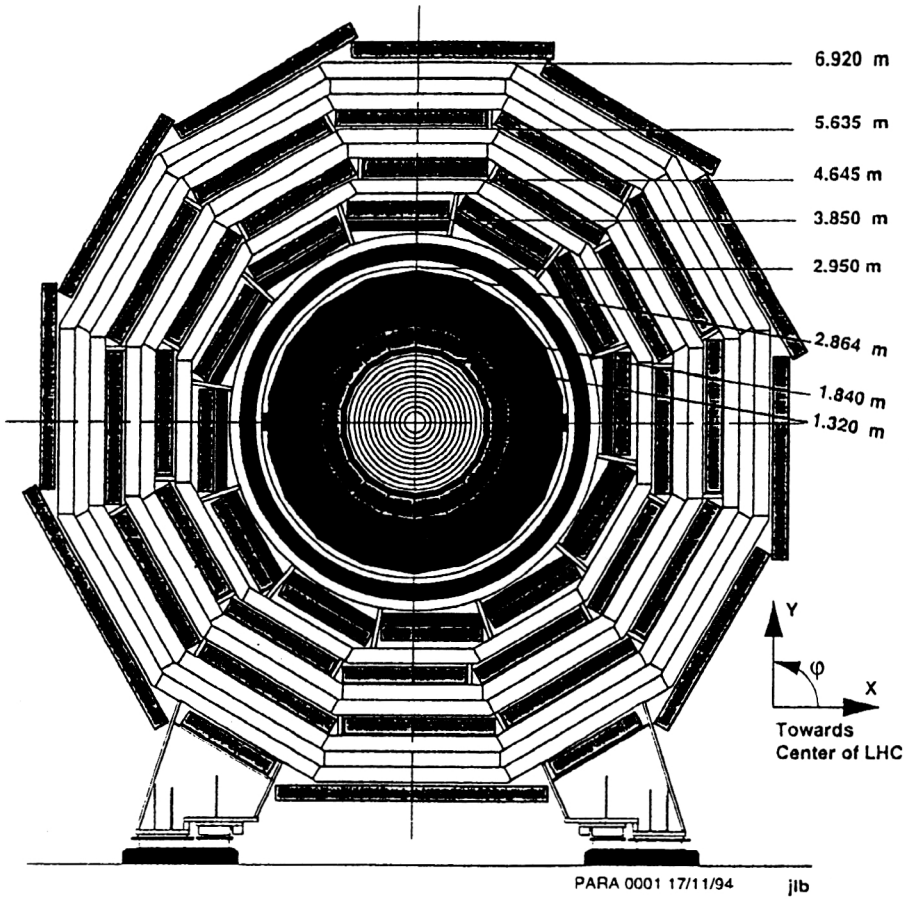

FIG. 2. Transverse view of the CMS detector.

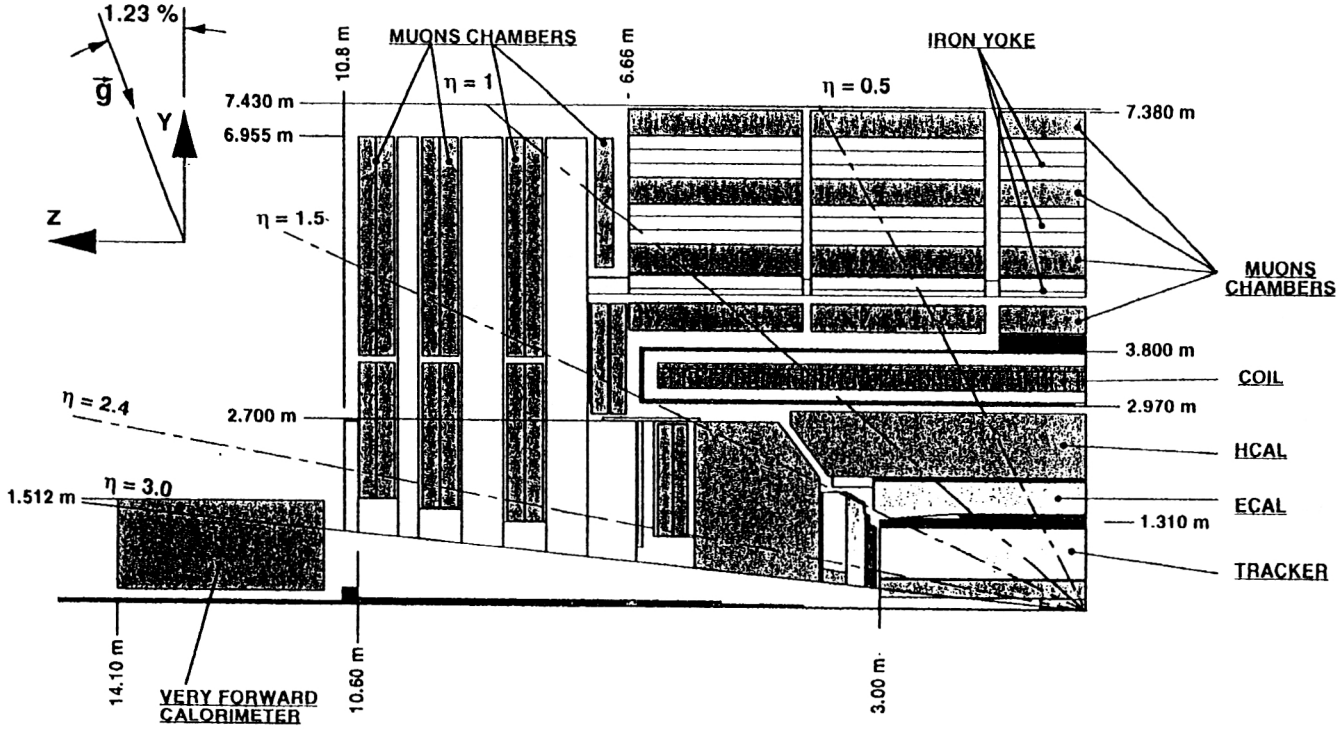

FIG. 3. Longitudinal view of the CMS detector.

ture of hadron collisions in many cases provides a reliable estimate of the cross sections. Two ingredients are required to compute the cross sections: the elementary cross sections and the parton distributions. It is straightforward to calculate the elementary cross sections, at least for low orders in perturbation theory. At a given scale, the parton distributions can be measured in deep inelastic lepton–hadron scattering. The evolution of these distributions to larger momentum scales is described by perturbative QCD.

As has been mentioned before, the main idea of the parton model is to regard a high-energy proton as a collection of quasifree partons which share its momentum. Thus, we consider a proton with momentum P as being made of partons carrying longitudinal momenta $x_i P$, where the momentum fractions x_i satisfy

$$0 \leqslant x_i \leqslant 1 \tag{8}$$

and

$$\sum_{\text{partons } i} x_i = 1. \tag{9}$$

The cross section for the reaction (6) is given by

$$d\sigma(a+b\to c+X) = \sum_{ij} f_i^{(a)}(x_a) f_j^{(b)}(x_b) d\hat{\sigma}(i+j\to c+X'), \tag{10}$$

where $f_i^{(a)}(x)$ is the number distribution of partons of species i. The summation runs over all contributing parton configurations. We denote the invariant mass of the $i-j$ system by

$$\sqrt{\hat{s}} = \sqrt{s\tau} \tag{11}$$

and its longitudinal momentum in the hadron–hadron c.m.s. by

$$p = x\sqrt{s}/2. \tag{12}$$

The kinematic variables $x_{a,b}$ of the elementary process are related to those of the hadronic process by

$$x_{a,b} = \frac{1}{2}\left[(x^2+4\tau)^{1/2} \pm x\right]. \tag{13}$$

The parton momentum fractions satisfy the relations

$$x_a x_b = \tau, \tag{14}$$

$$x_a - x_b = x. \tag{15}$$

The elementary parton model, as described here, disregards QCD strong-interaction effects. The most important modification of the naive parton model is due to QCD corrections to the parton distributions. In the leading logarithmic approximation[5] these corrections are process-independent and can be incorporated by the replacement

$$f_i^{(a)}(x_a) \to f_i^{(a)}(x_a Q^2). \tag{16}$$

There is some ambiguity in the choice of scale Q^2 for a particular process. It should be of the order of the subenergy $Q^2 \approx \hat{s}$. Knowledge of the next-to-leading corrections allows us to fix the scale Q^2. Usually, we shall neglect higher-order QCD corrections. Experience shows that in many cases inclusion of higher-order corrections increases the cross sections by a factor 1.5–2 (Ref. 5).

To calculate production cross sections for a hadron collider we need to know the parton distributions as functions of the scaling variable x and Q^2. For the study of a process with characteristic mass M, the parton distributions must be known for $Q^2 \approx M^2$ and $x \geqslant M^2/s$. The typical momentum fraction contributing to such a process is $x \approx M/\sqrt{s}$. We shall be interested in masses $M \geqslant O(100)$ GeV, so that for LHC we have $x \geqslant O(10^{-2})$ and $Q^2 \geqslant O(10^4)$ GeV^2. Although the distributions have not been measured at such values of Q^2, it is possible to obtain them by using the Altarelli–Parisi equation and the parton distributions at some scale Q_0^2. It is convenient to parametrize the distributions in a valence-plus-sea-plus-gluon form. The proton contains:

- up quarks: $u_v(x,Q^2)+u_s(x,Q^2)$;
- down quarks: $d_v(x,Q^2)+d_s(x,Q^2)$;
- up antiquarks $u_s(x,Q^2)$;
- down antiquarks: $d_s(x,Q^2)$;
- strange, charm, bottom, and top quarks and antiquarks: $q_s(x,Q^2)$;
- gluons: $G(x,Q^2)$.

The flavor quantum numbers of the proton are carried by the valence quarks. Those distributions must therefore satisfy the number sum rules

$$\int_0^u dx u_v(x,Q^2) = 2, \tag{17}$$

$$\int_0^1 dx d_v(x,Q^2) = 1. \tag{18}$$

The parton distributions are also constrained by the momentum sum rule

$$\int_0^1 dx x[u_v + d_v + G + 2(u_s + d_s + s_s + c_s + b_s + t_s)] = 1. \tag{19}$$

For protons, many sets of parton distributions exist on the market. These are obtained by fits to experimental data, constrained so that the Q^2 dependence is in accord with the standard QCD evolution equations. At present, the most popular set of parton distributions is CTEQ2L.[6] Also available in the PYTHIA program[7] are the EHLQ, DO, CTEQ2M, CTEQ2MS, CTEQ2MF, CTEQ2ML, and CTEQ2D sets of parton distributions. The Altarelli–Parisi equation for nonsinglet distributions reads

$$\frac{dp(x,Q^2)}{d\ln Q^2} = \frac{2\alpha_s(Q^2)}{3\pi}\int_x^1 dz\left[\frac{(1+z^2)p(y,Q^2)-2p(x,Q^2)}{1-z}\right] + \frac{\alpha_s(Q^2)}{\pi}\left[1+\frac{4\ln(1-x)}{3}\right]p(x,Q^2), \tag{20}$$

where

$$p(x,Q^2) = xu_v(x,Q^2) \text{ or } xd_v(x,Q^2) \tag{21}$$

and $y = x/z$. The evolution of the gluon momentum distribution

$$g(x,Q^2)=xG(x,Q^2) \tag{22}$$

is given by

$$\frac{dg(x,Q^2)}{d\ln Q^2}=\frac{\alpha_s(Q^2)}{\pi}\int_x^1 dz\left[\frac{3[zg(y,Q^2)-g(x,Q^2)]}{1-z}+\frac{3(1-z)(1+z^2)g(y,Q^2)}{z}+\frac{2}{3}\frac{1+(1-z)^2}{z}\sum_{\text{flavors: } q} y[q_v(y,Q^2)+2q_s(y,Q^2)]+\frac{\alpha_s(Q^2)}{\pi}\left[\frac{11}{4}-\frac{N_f}{6}+3\ln(1-x)\right]g(x,Q^2)\right], \tag{23}$$

where N_f is the number of flavors participating in the evolution at Q^2. The evolution of the momentum distributions of the light sea quarks

$$l(x,Q^2)=xu_s(x,Q^2) \text{ or } xd_s(x,Q^2) \text{ or } xs_s(x,Q^2) \tag{24}$$

is described by

$$\frac{dl(x,Q^2)}{d\ln Q^2}=\frac{2\alpha_s(Q^2)}{3\pi}\int_x^1 dz\left[\frac{(1+z^2)l(y,Q^2)-2l(x,Q^2)}{1-z}+\frac{3}{8}[z^2+(1-z^2)]g(y,Q^2)\right]+\frac{\alpha_s(Q^2)}{\pi}\left[1+\frac{4}{3}\ln(1-x)\right]l(x,Q^2). \tag{25}$$

For the evolution of the momentum distributions of heavy sea quarks

$$h(x,Q^2)=xc_s(x,Q^2) \text{ or } xb_s(x,Q^2) \text{ or } xt_s(x,Q^2) \tag{26}$$

the evolution equation reads[8]

$$\frac{dh(x,Q^2)}{d\ln Q^2}=\frac{2\alpha_s(Q^2)}{3\pi}\int_x^1 dz\left[\frac{(1+z^2)h(y,Q^2)-2h(x,Q^2)}{1-z}+\frac{3}{4\beta}\left[\frac{1}{2}-z(1-z)+\frac{M_q^2}{Q^2}\frac{(3-4z)z}{1-z}-\frac{16M_q^4z^2}{Q^4}\right]g(y,Q^2)-\frac{3M_q^2}{2Q^2}\left[z(1-3z)+\frac{4M_q^2z^2}{Q^2}\right]\ln\left(\frac{1+\beta}{1-\beta}\right)g(y,Q^2)\right]\theta(\beta^2)+\frac{\alpha_s(Q^2)}{\pi}[1+\ln(1-x)]h(x,Q^2), \tag{27}$$

where M_q is the heavy-quark mass and

$$\beta=[1-4M_q^2/Q^2(1-z)]^{1/2}. \tag{28}$$

The formula for the running effective strong coupling constant for massless quarks in the leading log approximation has the form

$$\alpha_s(Q^2)=\frac{12\pi}{(33-12N_f)\ln(Q^2/\Lambda^2)}. \tag{29}$$

We shall use the formula (29) for $N_f=4$. For the case of massive quarks the generalization of (29) takes the form

$$1/\alpha_s(Q^2)=\frac{25}{12\pi}\ln(Q^2/\Lambda^2)-\frac{1}{6\pi}\sum_{i=b,t,\ldots}\theta(Q^2-16M_i^2)\ln(Q^2/16M_i^2). \tag{30}$$

The parton distributions are necessary to calculate differential and total cross sections. It appears that the cross sections depend on a particular combination of structure functions and parton–parton luminosities. Specifically, the differential cross section for the reaction

$$a+b\to\alpha+\text{anything} \tag{31}$$

is given by

$$\frac{d\sigma}{d\tau}(a+b\to\alpha+X)=\sum_{ij}\frac{dL_{ij}}{d\tau}\hat{\sigma}(ij\to\alpha), \tag{32}$$

where $\hat{\sigma}(ij\to\alpha)$ is the cross section for the corresponding elementary process, $\tau=\hat{s}/s$, and

$$\frac{dL_{ij}}{d\tau}=\frac{1}{1+\delta_{ij}}\int_\tau^1 dx[f_i^{(a)}(x)f_j^{(b)}(\tau/x)+f_j^{(a)}(x)f_i^{(b)}(\tau/x)]/x. \tag{33}$$

Here $f_i^{(a)}(x)$ is the number distribution of partons of species i carrying momentum fraction x of hadron a. The hard-scattering processes that determine the study for interesting physics at LHC have a common asymptotic form prescribed by dimensional analysis:

$$\sigma(\hat{s})=c/\hat{s}. \tag{34}$$

For a strong-interaction process, such as jet pair production, c is typically of order $(\alpha_s/\pi)^2$. For a typical electroweak process, such as lepton pair production, c is approximately $(\alpha/\pi)^2$. Resonance-production cross sections are proportional to τ. Therefore, the quantity $(\tau/\hat{s})(dL/d\tau)$, which has the dimension of a cross section, provides a useful measure of the reach of a hadron collider at given energy and hadron–hadron luminosity.

3.2. Physics within the SM

3.2.1. Top-quark physics

Even at low initial luminosities of $10^{32}\,\text{cm}^{-2}\,\text{s}^{-1}$ approximately 6000 $t\bar{t}$ pairs would be produced per day at $m_t=170$ GeV, yielding about 100 reconstructed $t\bar{t}\to(l\nu b)\times(jjb)$ decays per day and about 10 clean isolated $e\mu$ pairs per day. The $t\to jjb$ decays provide an abundant event sample, which allows direct reconstruction of m_t, through the invariant mass of the 3-jet system. The conclusion is that the ultimate accuracy of ± 2 GeV may be achieved for $m_t=170$ GeV.[2]

Multilepton events from top-quark decays can also be used to extract an accurate measurement of m_t. The most promising method is to use two leptons from the same top-quark decay. For an integrated luminosity of $10^4\,\text{pb}^{-1}$, the

expected statistical uncertainty in the measurement of m_t, using this method, is approximately ± 0.5 GeV for $m_t = 170$ GeV. The total systematic uncertainty due to fragmentation effects will very likely be less than ± 2 GeV. The conclusion is that an accuracy better than ± 2 GeV may be achieved in this channel.

3.2.2. Higgs boson in the Weinberg–Salam model

The standard Weinberg–Salam model is the renormalizable model of strong and electroweak interactions. It has the gauge group $SU_c(3)\otimes SU(2)_L\otimes U(1)$ and the minimal Higgs structure consisting of one complex doublet of scalar particles. The spontaneous electroweak symmetry breaking $SU_c(3)\otimes SU_L(2)\otimes U(1)\to SU_c(3)\otimes U(1)$ due to a nonzero vacuum expectation value of the Higgs doublet provides the simplest realization of the Higgs mechanism,[9] which generates masses for the $W^{\pm}$ and Z gauge bosons and masses for the quarks and leptons. In this approach, the Goldstone bosons are generated by the dynamics of elementary scalar fields, and precisely one neutral Higgs scalar (the Higgs boson) remains in the physical spectrum. The Lagrangian of the Weinberg–Salam model consists of several parts:[10]

$$L_{\rm WS}=L_{\rm YM}+L_{\rm HYM}+L_{\rm SH}+L_f+L_{\rm Yuk}. \tag{35}$$

Here $L_{\rm YM}$ is the Yang–Mills Lagrangian without matter fields,

$$L_{\rm YM}=-\frac{1}{4}F^i_{\mu\nu}(W)F^{\mu\nu}_i(W)-\frac{1}{4}F^{\mu\nu}(W^0)F_{\mu\nu}(W^0)$$
$$-\frac{1}{4}F^a_{\mu\nu}(G)F^{\mu\nu}_a(G), \tag{36}$$

where $F^i_{\mu\nu}(W)$, $F^0_{\mu\nu}(G)$, $F_{\mu\nu}(W^0)$ are given by

$$F^i_{\mu\nu}(W)=\partial_\mu W^i_\nu-\partial_\nu W^i_\mu+g_2\epsilon^{ijk}W^j_\mu W^k_\nu, \tag{37}$$

$$F_{\mu\nu}(W^0)=\partial_\mu W^0_\nu-\partial_\nu W^0_\mu, \tag{38}$$

$$F^a_{\mu\nu}(G)=\partial_\mu G^a_\nu-\partial_\nu G^a_\mu+g_s f^{abc}G^b_\mu G^c_\nu, \tag{39}$$

in which $W^i_\mu W^0_\mu$ are the $SU_L(2)\otimes U(1)$ gauge fields, G^a_μ are the gluon fields, and ϵ^{ijk} and f^{abc} are the structure constants of the $SU(2)$ and $SU(3)$ gauge groups. The Lagrangian $L_{\rm HYM}$ describes the Higgs-doublet interaction with the $SU_L(2)\otimes U(1)$ gauge fields,

$$L_{\rm HYM}=(D_{L\mu}H)^+(D^\mu_L H), \tag{40}$$

where the covariant derivatives are given by

$$D_{L\mu}=\partial_\mu-ig_1\frac{Y}{2}W^0_\mu-ig_2\frac{\sigma^i}{2}W^i_\mu, \tag{41}$$

$$D_{R\mu}=\partial_\mu-ig_1\frac{Y}{2}W^0_\mu, \tag{42}$$

$$D^q_{L\mu}=\partial_\mu-ig_1\frac{Y}{2}W^0_\mu-ig_2\frac{\sigma^i}{2}W^i_\mu-ig_s t^a G^a_\mu, \tag{43}$$

$$D^q_{R\mu}=\partial_\mu-ig_1\frac{Y}{2}W^0_\mu-ig_s t^a G^a_\mu. \tag{44}$$

Here g_1 is the $U(1)$ gauge coupling constant, Y is the hypercharge determined by the relation $Q=\sigma_3/2+Y/2$, the σ^i are Pauli matrices, the t^a are $SU(3)$ matrices in the fundamental representation, and $H=\binom{H_1}{H_2}$ is the Higgs $SU(2)$ doublet with $Y=1$. The Lagrangian $L_{\rm SH}$ describing the Higgs-doublet self-interaction is

$$L_{SH}=-V_0(H)=M^2H^+H-\frac{\lambda}{2}(H^+H)^2, \tag{45}$$

where $H^+H=\Sigma_i H^*_i H_i$, and λ is the Higgs self-coupling constant. The Lagrangian L_f describes the interaction of fermions with gauge fields. Fermions constitute only doublets and singlets in $SU_L(2)\otimes U(1)$:

$$R_1=e_R,\quad R_2=\mu_R,\quad R_3=\tau_R, \tag{46}$$

$$L_1=\begin{pmatrix}\nu\\ e\end{pmatrix}_L,\quad L_2=\begin{pmatrix}\nu'\\ \mu\end{pmatrix}_L,\quad L_3=\begin{pmatrix}\nu''\\ \tau\end{pmatrix}_L, \tag{47}$$

$$R_{qIu}=(q_{Iu})_R(q_{1u}=u,\ q_{2u}=c,\ q_{3u}=t), \tag{48}$$

$$R_{qid}=(q_{id})_R(q_{1d}=d,\ q_{2d}=s,\ q_{3d}=b), \tag{49}$$

$$L_{qI}=\begin{pmatrix}q_{Iu}\\ V^{-1}_{Ii}q_{id}\end{pmatrix}_L, \tag{50}$$

where L and R denote left- and right-handed components of the spinors, respectively,

$$\psi_{R,L}=\frac{1\pm\gamma_5}{2}\psi, \tag{51}$$

and V_{il} is the Kobayashi–Maskawa matrix. The neutrinos are assumed to be left-handed and massless. The Lagrangian L_f has the form

$$L_f=\sum_{k=1}^{3}[i\bar L_k\hat D_L L_k+i\bar R_k\hat D_R R_k+i\bar L_{qk}\hat D^q_L L_{qk}$$
$$+i\bar R_{qku}\hat D^q_R R_{qku}+i\bar R_{qkd}\hat D^q_R R_{qkd}], \tag{52}$$

where $\hat D_L=\gamma^\mu D_{L\mu}$, $\hat D_R=\gamma^\mu D_{R\mu}$, $\hat D^q_L=\gamma^\mu D^q_{L\mu}$, and $\hat D^q_R=\gamma^\mu D^q_{R\mu}$. The Lagrangian $L_{\rm Yuk}$ generates fermion mass terms. Assuming that the neutrinos are massless, the Yukawa interaction of the fermions with the Higgs doublet has the form

$$L_{\rm Yuk}=-\sum_{k=1}^{3}[h_{lk}\bar L_k H R_k+h_{dk}\bar L_{dk}HR_{dk}$$
$$+h_{uk}\bar L_{uk}(i\sigma^2H^*)R_{uk}]+\text{H.c.} \tag{53}$$

The potential term $V_0(H)=-M^2H^+H+\lambda/2(H^+H)^2$ for $M^2>0$ gives rise to the spontaneous symmetry breaking. The doublet H acquires the nonzero vacuum expectation value

$$\langle H\rangle=\begin{pmatrix}0\\ \frac{v}{\sqrt2}\end{pmatrix}, \tag{54}$$

where $v=246$ GeV. In the unitary gauge, unphysical Goldstone massless fields are absent and the Higgs-doublet scalar field depends on a single physical scalar field $h(x)$ (Higgs field):

$$H(x)=\begin{pmatrix} 0 \\ \frac{v}{\sqrt{2}}+\frac{h(x)}{\sqrt{2}} \end{pmatrix}. \tag{55}$$

Because of spontaneous gauge symmetry breaking, gauge fields other than the photon field acquire masses. Diagonalization of the mass matrix gives

$$W_\mu^\pm=\frac{1}{\sqrt{2}}(W_\mu^1 \mp W_{mp}^2), \quad M_W=\frac{1}{2}g_2 v, \tag{56}$$

$$Z_\mu=\frac{1}{\sqrt{g_2^2+g_1^2}}(g_2 W_\mu^3-g_1 W_\mu^0), \quad M_Z=\frac{1}{2}\sqrt{g_2^2+g_1^2}\,v, \tag{57}$$

$$A_\mu=\frac{1}{\sqrt{q_2^2+g_1^2}}(g_1 W_\mu^3+g_2 W_\mu^0), \quad M_A=0, \tag{58}$$

where $W_\mu^\pm$, Z_μ are the charged and neutral electroweak bosons, and A_μ is the photon. It is convenient to introduce the rotation angle θ_W between (W^3,W^0) and (Z,A), which is called the Weinberg angle:

$$\sin\theta_W \equiv \frac{g_1}{\sqrt{g_1^2+g_2^2}} \tag{59}$$

Experimentally, $\sin^2\theta_W \approx 0.23$.[11] The formula for the electric charge e is

$$e=\frac{g_2 g_1}{\sqrt{g_2^2+g_1^2}}. \tag{60}$$

At the tree level the Higgs-boson mass is determined by the formula

$$m_h=\sqrt{2}M=\sqrt{\lambda}v. \tag{61}$$

The Lagrangian L_{Yuk} is responsible for the fermion mass generation. In the unitary gauge the Lagrangian L_{HYM} takes the form

$$L_{\text{HYM}}=\frac{1}{2}\partial^\mu h\partial_\mu h+M_W^2\left(1+\frac{h}{v}\right)^2 W_\mu^+ W^\mu+\frac{1}{2}M_Z^2\left(1+\frac{h}{v}\right)^2 Z^\mu Z_\mu. \tag{62}$$

The Yukawa Lagrangian in the unitary gauge can be written in the form

$$L_{\text{Yuk}}=-\sum_i m_{\psi_i}\left(1+\frac{h}{v}\right)\bar{\psi}_i\psi_i. \tag{63}$$

At present, the LEP1 lower bound on the Higgs-boson mass is[12]

$$m_i>63.5 \text{ GeV}. \tag{64}$$

In the standard Weinberg–Salam model there are several theoretical bounds on the Higgs-boson mass:

(i) Tree-level unitarity requires $m_h \leqslant 1$ TeV.[13]

(ii) The requirement that there is no Landau pole singularity for the effective Higgs self-coupling constant for energies up to 10^{14} GeV gives $m_h \leqslant 200$ GeV for $m_t \leqslant 200$ GeV.[14]

(iii) The vacuum-stability requirement leads to a lower bound on the Higgs-boson mass which depends on the top-quark mass.[15]

The renormalization-group equations for the effective coupling constants, disregarding all Yukawa coupling constants except the top-quark Yukawa coupling constant in the one-loop approximation, read

$$\frac{d\bar{g}_3}{dt}=-7\bar{g}_3^3, \tag{65}$$

$$\frac{d\bar{g}_2}{dt}=-\left(\frac{19}{6}\right)\bar{g}_2^3, \tag{66}$$

$$\frac{d\bar{g}_1}{dt}=\left(\frac{41}{6}\right)\bar{g}_1^3, \tag{67}$$

$$\frac{d\bar{h}_t}{dt}=\left(\frac{9\bar{h}_t^2}{2}-8\bar{g}_3^2-\frac{9\bar{g}_2^2}{4}-\frac{17\bar{g}_1^2}{12}\right)\bar{h}_t, \tag{68}$$

$$\frac{d\bar{\lambda}}{dt}=12\left(\bar{\lambda}^2+\left(\bar{h}_t^2-\frac{\bar{g}_1^2}{4}-\frac{3\bar{g}_2^2}{4}\right)\bar{\lambda}-\bar{h}_t^4+\frac{\bar{g}_1^4}{16}+\frac{\bar{g}_1^2\bar{g}_2^2}{8}+\frac{3\bar{g}_2^4}{16}\right), \tag{69}$$

$$t=\left(\frac{1}{16\pi^2}\right)\ln(\mu/m_Z). \tag{70}$$

Here $\bar{g}_3$, $\bar{g}_2$, and $\bar{g}_1$ are the $SU(3)$, $SU_L(2)$, and $U(1)$ gauge couplings, respectively, and $\bar{h}_t$ is the top-quark Yukawa coupling constant. In our estimates we took $m_t^{\text{pole}}=175$ GeV, $\bar{\alpha}_3(m_Z)=0.118$, $\bar{\alpha}_{em}^{-1}(m_Z)=127.9$, $\sin^2\theta_W(m_Z)=0.2337$, and $\alpha_i \equiv g_i^2/4\pi$. From the requirement that there is no Landau pole singularity for the Higgs self-coupling constant λ for scales up to $\Lambda=(10^3;10^4;10^6;10^8;10^{10};10^{12};10^{14})$ GeV (to be precise, we require that at the scale Λ the Higgs self-coupling constant is $\lambda^2(\Lambda)/4\pi \leqslant 1$) we have found the upper bounds on the Higgs-boson mass $m_h \leqslant (400;300;240;200;180;170;160)$GeV, respectively. Roughly speaking, the vacuum-stability bound comes from the requirement that the Higgs self-interaction coupling is nonnegative, $\bar{\lambda}(\mu)\geqslant 0$, for scales $\mu \leqslant M_s$. Here M_s is the scale up to which the standard model is applicable. Let us assume that at scales up to M_s the standard model works, and that at scales $M \geqslant M_s$ we have some supersymmetric extension of the standard model. It should be noted that the currently most popular minimal supersymmetric standard model (MSSM) predicts that the effective Higgs self-coupling constant for the standard model at the scale of supersymmetry breaking M_s must obey the inequality

$$0 \leqslant \bar{\lambda}(M_s)=(\bar{g}_1^2(M_s)+\bar{g}_2^2(M_s))(\cos(2\varphi))^2/4 \leqslant (\bar{g}_1^2(M_s)$$

TABLE I. Dependence of the Higgs-boson mass on the values of M_s, m_t^{pole}, and $k=0,1$. Everything except k is in GeV.

m_t^{pole}	165 $k=0$	165 $k=1$	170 $k=0$	170 $k=1$	175 $k=0$	175 $k=1$	180 $k=0$	180 $k=1$	185 $k=0$	185 $k=1$
$M_s=10^3$	69	111	74	114	78	117	83	120	88	123
$M_s=10^{3.5}$	81	117	86	120	92	124	98	128	104	132
$M_s=10^4$	89	121	95	125	101	130	108	134	114	139
$M_s=10^6$	105	129	113	135	121	141	129	147	137	153
$M_s=10^8$	112	132	120	138	129	147	138	152	146	159
$M_s=10^{10}$	115	133	124	140	133	147	142	154	151	161
$M_s=10^{12}$	117	134	126	141	136	147	145	154	154	161
$M_s=10^{14}$	118	134	127	141	132	148	147	156	156	164
$M_s=10^{16}$	118	134	128	141	138	148	148	156	158	164

$$+\bar{g}_2^2(M_s)/4. \tag{71}$$

Thus, the assumption that the standard Weinberg–Salam model originates from its supersymmetric extension with the supersymmetry broken at scale M_s allows us to obtain nontrivial information about the low-energy effective Higgs self-coupling constant in the effective potential $V=-M^2H^+H+(\lambda/2)(H^+H)^2$ and hence to obtain nontrivial information about the Higgs-boson mass. It should be noted that in nonminimal supersymmetric electroweak models, say, in the model with an additional gauge singlet σ, we have, as a result of the term $k\sigma H_1 i\tau_2 H_2$ in the superpotential, an additional term $k^2|H_1 i\tau_2 H_2|^2$ in the potential. As a result, our boundary condition for the Higgs self-coupling constant must be modified; specifically,

$$\bar{\lambda}(M_s)=\frac{1}{4}(\bar{g}_1^2(M_s)+\bar{g}_2^2(M_s))\cos^2(2\varphi)+\frac{1}{2}\bar{k}^2(M_s)\sin^2(2\varphi)\geqslant 0. \tag{72}$$

The boundary condition (72) depends on the unknown coupling constant $\bar{k}^2(M_s)$. However, it is very important to stress that for all nonminimal supersymmetric models broken down to the standard Weinberg–Salam model at scale M_s the effective Higgs self-coupling constant $\bar{\lambda}(M_s)$ is nonnegative, as a direct consequence of the nonnegativity of the effective potential in supersymmetric models. Therefore, the vacuum-stability requirement results naturally[16] if supersymmetry is broken at some high scale M_s and if at lower scales the standard Weinberg–Salam model is an effective theory. For MSSM with the boundary condition (71) for the Higgs self-coupling constant $\bar{\lambda}(M_s)$ we have integrated numerically the renormalization-group equations in the two-loop approximation. We also took into account the one-loop correction to the Higgs-boson mass [the running Higgs-boson mass $\bar{m}_h(\mu)=\sqrt{\bar{\lambda}(\mu)}v$ does not coincide with the pole Higgs-boson mass]. Our results for the Higgs-boson mass for various values of M_s and m_t^{pole} are presented in Table I. Here $k=0$ corresponds to the boundary condition $\bar{\lambda}(M_s)=0$, and $k=1$ corresponds to the boundary condition $\bar{\lambda}(M_s)=\frac{1}{4}(\bar{g}_1^2+\bar{g}_2^2)$.

The tree-level Higgs-boson couplings to gauge bosons and fermions can be deduced from the Lagrangians (62) and (63). Of these, hW^+W^-, hZZ, and $h\bar{\psi}\psi$ are most important for the phenomenology. The partial decay width into a fermion–antifermion pair is[10]

$$\Gamma(h\to\psi\bar{\psi})=\frac{G_F m_\psi^2 m_h N_c}{4\pi\sqrt{2}}\left(1-\frac{4m_\psi^2}{m_h^2}\right)^{3/2}, \tag{73}$$

where N_c is the number of fermion colors. For $m_h\leqslant 2m_W$ the Higgs boson decays mainly with ($\approx 90\%$ probability) into a b quark–antiquark pair and with $\approx 10\%$ probability into a τ lepton–antilepton pair. Higher-order QCD corrections can be effectively taken into account in Eq. (73) for the Higgs-boson decay into a b quark–antiquark pair by replacing the pole b-quark mass in Eq. (73) by the effective b-quark mass $\bar{m}_b(m_h)$. A Higgs boson with $m_h\geqslant 2M_W$ decays into pairs of gauge bosons with the partial widths

$$\Gamma(h\to W^+W^-)=\frac{G_F m_h^3}{32\pi\sqrt{2}}(4-4a_w+3a_w^2)(1-a_w)^{1/2}, \tag{74}$$

$$\Gamma(h\to Z^0Z^0)=\frac{G_F m_h^3}{64\pi\sqrt{2}}(4-4a_Z+3a_Z^2)(1-a_Z)^{1/2}, \tag{75}$$

where $a_W=4M_W^2/m_h^2$, and $a_Z=4M_Z^2/m_h^2$. In the heavy-Higgs mass regime ($2m_Z\leqslant m_h\leqslant 800$ GeV), the Higgs boson decays predominantly into gauge bosons. For example, for $m_h\gg 2m_Z$ we find that

$$\Gamma(h\to W^+W^-)=2\Gamma(h\to ZZ)\simeq\frac{G_F m_h^2}{8\pi\sqrt{2}}. \tag{76}$$

The m_h^3 behavior is the result of the longitudinal polarization states of the W and Z. As m_h becomes large, so does the coupling of h to the Goldstone bosons which have been eaten by the W and Z. However, the Higgs-boson decay width to a pair of heavy quarks grows only linearly in the Higgs-boson mass. Thus, for Higgs masses sufficiently far above $2m_Z$, the total Higgs-boson width is well approximated by ignoring the Higgs decay to $t\bar{t}$ and including only the two gauge-boson modes. For a heavy Higgs-boson mass we find

$$\Gamma_{\text{total}}(H)\simeq(0.48\ \text{TeV})\left(\frac{m_h}{1\ \text{TeV}}\right)^3. \tag{77}$$

It should be noted that a number of Higgs couplings are absent at the tree level but appear at the one-loop level. Among them, the couplings of the Higgs boson to two gluons and two photons are extremely important for Higgs-boson searches at supercolliders. The one-loop induced Higgs coupling to two gluons is due to t-quark exchange in the loop,[17] and it leads to an effective Lagrangian

$$L_{hgg}^{\text{eff}}=\frac{g_2\alpha_s}{24\pi m_W}\,hG^a_{\mu\nu}G^{a\mu\nu}. \tag{78}$$

Using the effective Lagrangian (78), we find

$$\Gamma(h\to gg)=\frac{g_2^2\alpha_s^2 m_h^3}{288\pi^3 m_W^2}. \tag{79}$$

Also very important is the one-loop induced Higgs-boson coupling to two photons due to W- and t-quark exchanges in the loop. The corresponding expression for the decay width of the Higgs boson into two photons is given in Ref. 18.

Consider now the search for the Higgs boson at supercolliders. For completeness let us start with LEP2. At LEP2 with total energy $\sqrt{s}=192$ GeV the dominant Higgs production process is $e^+e^-\to hZ$. The corresponding cross section at tree level is given by[19]

$$\sigma(e^+e^-\to hZ)=\frac{\pi\alpha^2\lambda^{1/2}(\lambda+12sM_Z^2)[1+(1-4\sin^2\theta_W)^2]}{192s^2\sin^4\theta_W\cos^4\theta_W(s-M_Z^2)^2}, \tag{80}$$

where $\lambda\equiv(s-m_h^2-M_Z^2)^2-4m_h^2M_Z^2$. We see that, for a fixed value of m_h, the cross section is maximal for $\sqrt{s}\approx m_Z+\sqrt{2}m_h$. For $L_t=500\ \text{pb}^{-1}$ we expect to observe Higgs bosons using the signature $Z\to\nu\bar{\nu}$, $h\to b\bar{b}$ for masses up to M_Z. Note that the region $m_h\simeq M_Z$ is particularly troublesome due to the $e^+e^-\to ZZ$ background. Both ZZ and hZ lead to four-fermion states. However, these states can be separated by making use of the fact that $\text{Br}(h\to b\bar{b})\approx 90\%$, compared with $\text{Br}(Z\to b\bar{b})\approx 20\%$. Given sufficient energy and luminosity, and a vertex detector that can tag b-quark jets with high efficiency, it would be possible to discover a Higgs boson if it is degenerate in mass with the Z boson.

At LHC the dominant mechanism for Higgs-boson production is gluon–gluon fusion. In addition, WW fusion becomes important for a heavy Higgs boson. The cross section for Higgs-boson production due to gluon–gluon fusion has the form

$$\frac{d\sigma}{dy}(AB\to h+X)=\frac{\pi^2\Gamma(h\to gg)}{8m_h s}\,G_A(x_a,m_h^2)G_B(x_b,m_h^2), \tag{81}$$

where G_A and G_B are the gluon distribution functions in hadrons A and B, respectively, and

$$x_a=\frac{m_h e^y}{\sqrt{s}},\qquad x_b=\frac{m_h e^{-y}}{\sqrt{s}}, \tag{82}$$

$$y=\frac{1}{2}\ln\left(\frac{E_h+p_{3h}}{E_h-p_{3h}}\right). \tag{83}$$

The rapidity y is defined in terms of the Higgs-boson energy and the longitudinal momentum is defined in the laboratory frame.

3.2.3. Search for the standard Higgs boson at CMS

The search for $h\to\gamma\gamma$. One of the most important reactions for the search for Higgs boson at LHC is

$$pp\to(h\to\gamma\gamma)+\dots\ . \tag{84}$$

This reaction is the most promising one for the search for Higgs bosons in the most interesting region $90\ \text{GeV}\leqslant m_h\leqslant 140\ \text{GeV}$.

The key features that enable the CMS detector to give clear, two-photon mass peaks, significantly above the background throughout the intermediate mass range, are:

(i) An electromagnetic calorimeter with excellent energy resolution (this requires calibration to high precision, which in turn requires a good inner tracking system).

(ii) Large acceptance (the precision electromagnetic calorimetry extends to $|\eta|=2.5$), adequate neutral-pion rejection, and (at high luminosity) good measurement of the photon direction. This requires fine lateral segmentation and a preshower detector.

(iii) Use of a powerful inner tracking system for isolation cuts.

The product of the cross section and the branching ratio has been estimated to be $\sigma\ \text{Br}(h\to\gamma\gamma)=76$ fb (68 fb) for $m_h=110$ (130) GeV, and the uncertainty in the cross-section calculation is 30–50%. The imposition of cuts ($|\eta|\leqslant 2.5$, $p_T^{\gamma_1}\geqslant 40$ GeV, $p_T^{\gamma_2}\geqslant 25$ Gev) makes it possible to decrease the background to a reasonable level. The jet background is reduced by imposing an isolation cut, which also reduces the bremsstrahlung background. A photon is said to be isolated if there is no charged track or electromagnetic shower with a momentum greater than 2.5 GeV within a region $\Delta R\leqslant 0.3$ around it. The photons from the decay of π^0, with the relevant transverse momenta, are separated in the calorimeter by a lateral distance of the order of 1 cm. An efficiency of 64% was assumed for reconstruction of each photon (i.e., 41% per event). The crystal calorimeter was assumed to have an energy resolution $\Delta E/E=0.02/\sqrt{E}\oplus 0.005\oplus 0.2/E$ in the barrel and $\Delta E/E=0.05/\sqrt{E}\oplus 0.005\oplus 0.2/E$ in the endcap, where there is a preshower detector. At high luminosity, a barrel preshower detector covers $|\eta|<1.1$, resulting in a resolution $\Delta E/E=0.05/\sqrt{E}\oplus 0.005\oplus 0.2/E$ and an ability to measure the photon direction with resolution $\Delta\alpha=40\ \text{mrad}/\sqrt{E}$ in this region.

The background to the process $h\to\gamma\gamma$ can be divided into three parts:

1. Prompt diphoton production from quark-annihilation and gluon-fusion diagrams—the irreducible background.

2. Prompt diphoton production from bremsstrahlung from the outgoing quark line in the QCD Compton diagram.

3. Background from jets, where an electromagnetic energy deposit originates from the decay of neutral hadrons in a jet from 1 jet+1 prompt photon.

The signal significance $\sigma = N_S/\sqrt{N_B}$ is estimated to be 7σ (9σ) for $m_h = 110$ (130) GeV and for low luminosity $L_{\text{low},t} = 3\times 10^4$ pb^{-1}, and 10σ (13σ) for $m_h = 110$ (130) GeV and for high luminosity $L_{\text{high},t} = 10^5$ pb^{-1}. The general conclusion is that at the 5σ level it would be possible to discover the Higgs boson for 95 GeV$\leq m_h \leq$145 GeV at low luminosity, while at high luminosity the corresponding mass interval for discovery of the Higgs boson is 85 GeV$\leq m_h \leq$150 GeV.

Search for $h\to\gamma\gamma$ in association with high-E_T jets. The possibility of the search for $h\to\gamma\gamma$ with a large E_T jet makes it possible to improve the signal-to-background ratio. There are several sources of such Higgs+jet events. One is the next-to-leading-order corrections to $gg\to h$ with hard gluons. Others are associated production of $\bar{t}th$, Wh, Zh, and the WW and Zh fusion mechanisms.

The cuts that provide optimal sensitivity are:[1]

(i) Two isolated photons are required, with $p_t^{\gamma_1} \geq 40$ GeV, $p_t^{\gamma_2} \geq 60$ GeV, $|\eta| \leq 2.5$, and $p_t^{\gamma\gamma} \geq 50$ GeV.

(ii) The number of jets is ≥ 2, $E_t^{\text{jet}} \geq 40$ GeV for central jets ($|\eta| \leq 2.4$), and $E^{\text{jet}} \geq 800$ GeV for forward jets ($2.4 \leq |\eta| \leq 4.6$).

(iii) Photons are isolated, with no charged or neutral particles with $p_t \geq 2$ GeV within a cone $\Delta R \leq 0.3$ around the direction of each photon.

(iiii) γ-jet isolation: $\Delta R(\gamma,\text{jet}) > 1.5$ (to suppress the bremsstrahlung contribution).

The calculations give encouraging results; i.e., for $L_{\text{high},t} = 1.6\times 10^5$ pb^{-1} it would be possible to discover the Higgs boson for 70 GeV$\leq m_h \leq$150 GeV with $\geq 7\sigma$ signal significance. Note that the background is not only much smaller in magnitude than in the inclusive $h\to\gamma\gamma$ search, but it is also peaked at higher masses, away from the most difficult region $m(\gamma\gamma) \leq 90$ GeV.

$h\to\gamma\gamma$ in association with Wh and $\bar{t}th$ production. The $Wh\to l\gamma\gamma+X$ and $\bar{t}th\to l\gamma\gamma+X$ final states are other promising signatures for the Higgs-boson search. The production cross section is smaller than for inclusive $h\to\gamma\gamma$ by a factor ≈ 30. However, the isolated hard lepton from the W and t decays makes it possible to obtain a strong background reduction and to indicate the primary vertex at any luminosity. The main backgrounds are $W\gamma\gamma$, $W\gamma$+jet, $W+2$ jets, $t\bar{t}\gamma\gamma$, $t\bar{t}\gamma$, $t\bar{t}$, $b\bar{b}$, $c\bar{c}$, and $t\bar{b}$, with a real lepton in the final state and one or two jets faking photons due to hard bremsstrahlung. For 80 GeV$\leq m_h \leq$120 GeV and $L_{\text{high},t} = 1.6\times 10^5$ pb^{-1} the signal significance is better than 6σ.

$h\to ZZ^*(ZZ)\to 4$ leptons. The search for the standard Higgs boson using the reaction $h\to ZZ^*(ZZ)\to 4$ leptons is possible for a broad mass range, 130 GeV$\leq m_h \leq$800 GeV. Below $2M_Z$ the event rate is small and the background reduction is more difficult, as one of the Z's is off the mass shell. In this mass region the width of the Higgs boson is small: $\Gamma_h < 1$ GeV. The significance of the signal is proportional to the mass resolution, and so the lepton momentum resolution is of decisive importance. The geometrical and kinematic acceptance for leptons is also very important in these channels[1] in the $m_h < 2M_Z$ mass region; the main backgrounds are from $t\bar{t}$, $Zb\bar{b}$, and ZZ^*. The ZZ^* background is irreducible and peaks sharply near the ZZ threshold. The $Zb\bar{b}$ background cannot be reduced by a Z mass cut, but it can be suppressed by lepton isolation. The $t\bar{t}$ background can be reduced by a Z mass cut and by isolation cuts. The standard event cuts were choosen as follows:[1] one electron with $p_t > 20$ GeV, one with $p_t > 15$ GeV, and the other two with $p_t > 10$ GeV, all within $|\eta| < 2.5$. For muons, the corresponding p_t cuts are 20, 10, and 5 GeV in the rapidity range $|\eta| < 2.4$. For $m_h = 130$ GeV the total (kinematic and geometrical) acceptance for the four-electron channel is 22%, and for the four-muon channel it is 42%. For $m_h = 170$ GeV these acceptances increase to 38% and 48%, respectively. To select $h\to ZZ^*$ events and suppress the large $t\bar{t}$ background, one of the e^+e^- or $\mu^+\mu^-$ pairs was assumed to be within $\pm 2\sigma_Z$ of the Z mass. There is a fraction of events where both Z's are off-shell. This effect results in a 24% loss for $m_h = 130$ GeV, decreasing to 12% for $m_h = 170$ GeV. The M_Z cut reduces the $t\bar{t}$ background by a factor of 11 in the $Z\to\mu^+\mu^-$ channel and by a factor of 5 in the $Z\to e^+e^-$ channel. For two softer leptons, $M(ll) > 12$ GeV is also required.

For the region 130 GeV$\leq m_h \leq$180 GeV it would be possible, for $L_{\text{high},t} = 10^5$ pb^{-1}, to discover the Higgs boson with $\geq 5\sigma$ signal significance, except in a narrow mass region near 170 GeV. For $m_h \geq 180$ GeV the $h\to ZZ\to 4l^{\pm}$ channel is sensitive for low luminosity 10^4 pb^{-1} from $2m_Z$ to 400 GeV. The main background here is nonresonant ZZ production. The conclusion is that even at low luminosity $L_{\text{low},t} = 10^4$ pb^{-1} it would be possible to discover the Higgs boson for $2m_Z \leq m_h \leq 400$ GeV.

The use of the channels $h\to llv\nu$, $h\to WW\to l\nu jj$, and $h\to ZZ\to lljj$. The channel $h\to llv\nu$ has a branching ratio six times larger than for $h\to 4l^{\pm}$. The main background comes from ZZ, ZW, $t\bar{t}$, and Z+jets. The chosen cuts are:

1. $E_t^{\text{miss}} \geq 100$ GeV.
2. Two leptons are required, with $p_t \geq 20$ GeV, $|\eta| \leq 1.8$, and $p_t^{ll} \geq 60$ GeV.
3. $|M_Z - M_{ll}| \leq 6$ GeV.
4. No other isolated leptons with $p_t \geq 6$ GeV.
5. No central jets with $E_t \geq 150$ GeV.
6. No jets back-to-back with leptons (the cosine of the angle between the momentum of the lepton pair and the sum of the momenta of the jets is ≥ -0.8).
7. E_t^{miss} vector back-to-back with the lepton pair (the cosine of the angle in the transverse plane between the two-lepton momentum and the missing transverse momentum is ≤ 0.8).

The conclusion is that by using this mode it would be possible to discover the Higgs boson in the interval 400 GeV$\leq m_h \leq$(800–900) GeV.

The channels $h\to WW\to l\nu jj$ and $h\to ZZ\to lljj$ are important in the $m_h \approx$1-TeV mass range, where the large $W,Z\to q\bar{q}$ branching ratios must be used. In addition, high lepton pairs with $m_{ll} \approx M_Z$ for $h\to ZZ$, or a high-p_t lepton pair plus large E_t^{miss} for $h\to WW$, must be used. Two hard jets from the hadronic decays of Z/W with $m_{jj} \approx M_{Z/W}$ are also required. The backgrounds are Z+jets, ZW, WW, $t\bar{t}$, WW, WZ. For $m_h \approx 1$ TeV the Higgs boson is very broad ($\Gamma_h \approx 0.5$ TeV and the WW/ZZ fusion mechanism represents

about 50% of the total production cross section), and therefore a forward-region signature is essential. The appropriate cuts are:

(i) $E_t^{\text{miss}} \geqslant 150$ GeV, $p_t^l \geqslant 150$ GeV, $p_t^W \geqslant 300$ GeV for $h \to WW$, or $p_t^l \geqslant 50$ GeV, $p_t^Z \geqslant 50$ GeV, $p_t^Z \geqslant 150$ GeV, $|m_Z - m_{ll}| \leqslant 10$ GeV for $h \to ZZ$.

(ii) $|m_{jj} - m_{W/Z}| \leqslant 15$ GeV for a central jet pair.

(iii) $E_t^{\text{jet}} \geqslant 10$ GeV, $E^{\text{jet}} \geqslant 400$ GeV, $|\eta| \geqslant 2.4$ for the two forward tagging jets.

The main conclusion is that the use of the reactions $h \to WW \to l\nu jj$ and $h \to ZZ \to lljj$ makes it possible to discover a heavy Higgs boson with mass up to 1 TeV for $L_{\text{high},t} = 10^5$ pb^{-1}.

3.2.4. B physics in the SM

General comments. The main task of B-physics investigations at LHC is the observation of CP violation. For such a measurement, high statistics are important, since the useful decay rates have branching ratios 10^{-4}–10^{-7}. At LHC, 10^{12}–10^{13} $b\bar{b}$ pairs will be produced per year, and so the main problem here is to trigger and select the interesting modes. The violation of CP symmetry is one of the most intriguing aspects of high-energy physics. So far, there has been only a single measurement of a CP-violation parameter: the measurement of ϵ_K in K decays. The standard model description of CP violation is very predictive: all CP-violating effects are related to the phase δ of the Cabibbo–Kobayashi–Maskawa (CKM) matrix. Note that in the standard model the θ term

$$\theta \frac{\alpha_s}{4\pi} \text{Tr} G_{\mu\nu} \tilde{G}^{\mu\nu} \tag{85}$$

in the QCD Lagrangian violates CP symmetry.[20] The θ term gives a nonzero contribution to the electric dipole moment of the neutron.[20] The current experimental bound on the electric dipole moment of the neutron, $|d_n| \leqslant 1.1 \times 10^{-25}\ e \cdot \text{cm}$, implies that $|\theta| \leqslant 10^{-9}$, which corresponds to an extreme fine-tuning of a parameter of the QCD Lagrangian. Therefore, the prospects are good that detailed investigation of CP violation in B decays will provide important information about the possible mechanisms of CP violation.

Let us briefly describe the P, C, and CP transformations.[21] The parity transformation is a space-time transformation, under which $t \to -t$ and $\mathbf{x} \to -\mathbf{x}$. It changes the sign of the momenta, $\mathbf{p} \to -\mathbf{p}$, leaving the spins unchanged. For pseudoscalar mesons P and $\tilde{P}$, the parity transformation could be defined as

$$\hat{P}|P(\mathbf{p})\rangle = -|P(-\mathbf{p})\rangle, \tag{86}$$

$$\hat{P}|\tilde{P}(\mathbf{p})\rangle = -|\tilde{P}(-\mathbf{p})\rangle. \tag{87}$$

Charge conjugation relates particles and antiparticles, leaving all space-time coordinates unchanged; i.e.,

$$\hat{C}|P(\mathbf{p})\rangle = |\tilde{P}(\mathbf{p})\rangle, \tag{88}$$

$$\hat{C}|\tilde{P}(\mathbf{p})\rangle = |P(\mathbf{p})\rangle. \tag{89}$$

The combined CP transformation acts on pseudoscalar mesons in the following way:

$$\hat{C}\hat{P}|P(\mathbf{p})\rangle = -|\tilde{P}(-\mathbf{p})\rangle, \tag{90}$$

$$\hat{C}\hat{P}|\tilde{P}(\mathbf{p})\rangle = -|P(-\mathbf{p})\rangle. \tag{91}$$

For neutral P^0 and $\tilde{P}^0$ mesons one can construct the CP eigenstates

$$|P_1^0\rangle = \frac{1}{\sqrt{2}}(|P^0\rangle - |\tilde{P}^0\rangle),$$

$$|P_2^0\rangle = \frac{1}{\sqrt{2}}(|P^0\rangle + |\tilde{P}^0\rangle),$$

which obey the relations

$$\hat{C}\hat{P}|P_1^0\rangle = |P_1^0\rangle,$$

$$\hat{C}\hat{P}|P_2^0\rangle = -|P_2^0\rangle.$$

CP violation in the standard model. The standard-model gauge group $SU_C(3) \otimes SU_L(2) \otimes U(1)$ is spontaneously broken down to $SU_C(3) \otimes U(1)$, as a result of the nonzero vacuum expectation value of the Higgs doublet. This gives masses to the W and Z bosons, as well as to the quarks and leptons. The quark masses arise from the Yukawa couplings to the Higgs doublet. The Yukawa interactions are written in terms of the weak eigenstates q' of the quark fields. After the electroweak symmetry breaking the quark fields are redefined so as to obtain the mass terms in the canonical way. In the weak basis these charged-current interactions have the form

$$L_{\text{int}} = -\frac{g_2}{\sqrt{2}} (\bar{u}_L', \bar{c}_L', \bar{t}_L') \gamma^\mu \begin{pmatrix} d_L' \\ s_L' \\ b_L' \end{pmatrix} W_\mu^+ + \text{H.c.} \tag{92}$$

In terms of the mass eigenstates q, L_{int} can be rewritten in the form

$$L_{\text{int}} = -\frac{g_2}{\sqrt{2}} (\bar{u}_L, \bar{c}_L, \bar{t}_L) \gamma^\mu V_{\text{CKM}} \begin{pmatrix} d_L \\ s_L \\ b_L \end{pmatrix} W_\mu^+ + \text{H.c.} \tag{93}$$

The CKM mixing matrix V_{CKM} is a unitary matrix in flavor space. In the case of three generations, V_{CKM} can be parametrized by three Euler angles and six phases, five of which can be eliminated by redefinition of the left-handed quark fields. Thus, three angles θ_{ij} and one observable complex phase δ remain in the quark mixing matrix.[21]

The "standard parametrization" of the CKM matrix is

$$V_{\mathrm{CKM}}=\begin{pmatrix} c_{12}c_{13} & s_{12}c_{13} & s_{13}e^{-i\delta} \\ -s_{12}c_{23}-c_{12}s_{23}s_{13}e^{i\delta} & c_{12}c_{23}-s_{12}s_{23}s_{13}e^{i\delta} & s_{23}c_{13} \\ s_{12}s_{23}-c_{12}c_{23}s_{13}e^{i\delta} & -c_{12}s_{23}-s_{12}c_{23}s_{13}e^{i\delta} & c_{23}c_{13} \end{pmatrix}. \tag{94}$$

Here $c_{ij}=\cos(\theta_{ij})$ and $s_{ij}=\sin(\theta_{ij})$. The imaginary part of the mixing matrix is necessary to describe CP violation in the standard model. In general, CP is violated in flavor-changing decays if there is no degeneracy of any two quark masses and if $J_{CP}\neq 0$, where

$$J_{CP}=|\mathrm{Im}(V_{ij}V_{kl}V_{il}^{*}V_{kj}^{*}|; \quad i\neq k, \quad j\neq l. \tag{95}$$

It can be shown that all CP-violating amplitudes in the standard model are proportional to J_{CP}.

For many applications it is more convenient to use an approximate parametrization of the CKM matrix (the Wolfenstein parametrization):[22]

$$V_{\mathrm{CKM}}\simeq\begin{pmatrix} 1-\frac{\lambda^2}{2} & \lambda & A\lambda^3(\rho-i\eta) \\ -\lambda & 1-\frac{\lambda^2}{2} & A\lambda^2 \\ A\lambda^3(1-\rho-i\eta) & -A\lambda^2 & 1 \end{pmatrix} + O(\lambda^4). \tag{96}$$

One finds that

$$J_{CP}\simeq A^2\eta\lambda^6\simeq 1.1\times 10^{-4}\cdot A^2\eta. \tag{97}$$

The two Wolfenstein parameters λ and A are experimentally well determined:[23]

$$\lambda=|V_{us}|=0.2205\pm 0.0018, \tag{98}$$

$$A=\left|\frac{V_{cb}}{V_{us}^2}\right|=0.80\pm 0.04. \tag{99}$$

A simple way to take into account the implications of the unitarity of the CKM matrix is provided by the so-called unitarity triangle, which uses the fact that the unitarity equation

$$V_{ij}V_{ik}^{*}=0 \quad (j\neq k) \tag{100}$$

can be represented as the equation of a closed triangle in the complex plane. There are six such triangles with the same area:[24]

$$|A_{\Delta}|=\frac{1}{2}J_{CP}. \tag{101}$$

Most useful from the phenomenological point of view is the triangle relation

$$V_{ud}V_{ub}^{*}+V_{cd}V_{cb}^{*}+V_{td}V_{tb}^{*}=0, \tag{102}$$

which determines a triangle with angles α, β, γ ($\alpha+\beta+\gamma=\pi$). The present fit to the data for the triangle gives $\sin(2\alpha)\approx 0.7$, $\sin(2\beta)\approx 0.5$, $\sin(\gamma)\approx 0.9$.

Direct CP violation in weak decays. Consider two decay processes related to each other by a CP transformation. Let P and $\tilde{P}$ be CP-conjugate pseudoscalar meson states, and f and $\tilde{f}$ be some CP-conjugate final states:

$$\hat{C}\hat{P}|P\rangle=e^{i\phi_P}|\tilde{P}\rangle, \quad \hat{C}\hat{P}|f\rangle=e^{i\phi_f}|\tilde{f}\rangle. \tag{103}$$

The phases ϕ_P and ϕ_f are arbitrary. The CP-conjugate amplitudes, A and $\bar{A}$, can be written as

$$A=\langle f|H|P\rangle=\sum_i A_i e^{i\delta_i}e^{i\phi_i}, \tag{104}$$

$$\bar{A}=\langle\tilde{f}|H|\tilde{P}\rangle=e^{i(\phi_P-\phi_f)}\sum_i A_i e^{i\delta_i}e^{-ig f_i}, \tag{105}$$

where H is the effective Hamiltonian for weak decays, and the A_i are real partial amplitudes. The weak phases ϕ_i are parameters of the CP-violating Lagrangian. They appear in the electroweak sector of the theory and enter into a and $\bar{A}$ with opposite signs. The strong phases δ_i appear in the scattering amplitudes even if the Lagrangian is CP-invariant, and they enter into A and $\bar{A}$ with the same sign. It appears that the ratio

$$\left|\frac{\bar{A}}{A}\right|=\left|\frac{\Sigma_i A_i e^{i\delta_i}e^{i\phi_i}}{\Sigma_i A_i e^{i\delta_i}e^{-i\phi_i}}\right| \tag{106}$$

is independent of the phase conventions. The inequality

$$\left|\frac{\bar{A}}{A}\right|\neq 1 \tag{107}$$

implies direct CP violation, which comes from the interference of the decay amplitudes leading to the same final states, and this requires at least two partial amplitudes that differ in both the weak and strong phases.

Since mixing is unavoidable in neutral meson decays, the best way to observe direct CP violation is in the decays of charged mesons. The CP asymmetry is defined in the standard way:

$$a_f=\frac{\Gamma(P^{+}\to f)-\Gamma(P^{-}\to\bar{f})}{\Gamma(P^{+}\to f)+\Gamma(P^{-}\to\bar{f})}=\frac{1-\left|\frac{\bar{A}}{A}\right|^2}{1+\left|\frac{\bar{A}}{A}\right|^2}. \tag{108}$$

We must consider nonleptonic decays, since leptonic and semileptonic decays are usually dominated by a single diagram, and the complex phases cancel. Nonleptonic decays can receive both tree and penguin contributions.[25] Penguin diagrams typically involve weak phases other than tree diagrams. To obtain large interference effects, one needs partial amplitudes with similar amplitude. Therefore, it is necessary to look for decays in which the tree contribution is suppressed by small CKM parameters that compensate for the loop suppression of the penguin diagrams. Another possibil-

ity is to consider tree-forbidden decays, which can only proceed through penguin diagrams. Examples are $B^{\pm}\to K^{\pm}K$, $B^{\pm}\to K^{\pm}\phi$, $B^{\pm}\to K^{*\pm}\gamma$, and $B^{\pm}\to\rho^{\pm}\gamma$. At present, there is no experimental evidence for direct CP violation.

Indirect CP violation in the mixing of neutral mesons. The neutral mesons P^0 and $\widetilde{P}^0$ can mix via common decay channels:

$$P^0\leftrightarrow X\leftrightarrow\widetilde{P}^0. \tag{109}$$

An arbitrary neutral meson state can be written as a superposition of the eigenstates $a|P^0\rangle+b|\widetilde{P}^0\rangle$, which obey the Schrödinger equation

$$i\frac{d(a,b)}{dt}=\mathbf{H}(a,b)=\left(\mathbf{M}-\frac{i}{2}\mathbf{\Gamma}\right)(a,b), \tag{110}$$

where $\mathbf{M}$ and $\mathbf{\Gamma}$ are Hermitian 2×2 matrices. Since the Hamiltonian operator $\mathbf{H}$ is not Hermitian, its eigenstates

$$|P_{1,2}\rangle=p|P^0\rangle\pm q|\widetilde{P}^0\rangle,\quad |p^2|+|q^2|=1 \tag{111}$$

are not orthogonal, and the eigenvalues,

$$\mu_j=M_j-\frac{i}{2}\Gamma_j,\quad j=1,2, \tag{112}$$

are complex. The time evolution of the states P_i is given by

$$|P_i(t)\rangle=e^{-iM_it}e^{-1/2\Gamma_it}|P_i(0)\rangle. \tag{113}$$

It can be shown that the ratio

$$\left|\frac{q}{p}\right|^2=\left|\frac{M_{12}^*-\frac{i}{2}\Gamma_{12}^*}{M_{12}-\frac{i}{2}\Gamma_{12}}\right|^2 \tag{114}$$

is independent of the phase conventions. The condition $|q/p|\neq1$ implies CP violation due to the difference of the flavor eigenstates from the CP eigenstates. The following relations are valid:

$$(\Delta m)^2-\frac{1}{4}(\Delta\Gamma)^2=4|M_{12}|^2-|\Gamma_{12}|^2, \tag{115}$$

$$\Delta m\cdot\Delta\Gamma=4\,\mathrm{Re}(M_{12}\Gamma_{12}^*), \tag{116}$$

$$\frac{q}{p}=-\frac{1}{2}\frac{\Delta m-\frac{i}{2}\Delta\Gamma}{M_{12}-\frac{i}{2}\Gamma_{12}}=-2\frac{M_{12}^*-\frac{i}{2}\Gamma_{12}^*}{\Delta m-\frac{i}{2}\Delta\Gamma}, \tag{117}$$

where $\Delta m=m_2-m_1$, and $\Delta\Gamma=\Gamma_2-\Gamma_1$. An alternative notation is to define $\widetilde{\epsilon}$ in such a way that

$$p=\frac{1+\widetilde{\epsilon}}{\sqrt{2(1+|\widetilde{\epsilon}|^2)}},\quad q=\frac{1-\widetilde{\epsilon}}{\sqrt{2(1+|\widetilde{\epsilon}|^2)}},\quad \frac{q}{p}=\frac{1-\widetilde{\epsilon}}{1+\widetilde{\epsilon}}. \tag{118}$$

Consider first the kaon system. We define the "short-lived" and "long-lived" neutral-kaon states as $K_S=K_1$ and $K_L=K_2$. Experimentally,

$$\Delta m_K=m_L-m_S=(3.510\pm0.018)\times10^{-15}\ \text{GeV}, \tag{119}$$

$$\Delta\Gamma_K=\Gamma_L-\Gamma_S=-(7.361\pm0.010)\times10^{-15}\ \text{GeV}. \tag{120}$$

We define

$$\frac{\Gamma_{12}^*}{M_{12}^*}=-\left|\frac{\Gamma_{12}}{M_{12}}\right|e^{i\varphi_{12}}. \tag{121}$$

From the last definition we find

$$\left|\frac{q}{p}\right|_K-1\simeq-2\,\mathrm{Re}(\widetilde{\epsilon}_K)\simeq-\varphi_{12}=O(10^{-3}). \tag{122}$$

For B-meson systems, decay channels common to B^0 and $\widetilde{B}^0$, which are responsible for the difference $\Delta\Gamma_B$, are known to have branching ratios of order 10^{-3} or less. Hence $|\Delta\Gamma_B/\Gamma_B|\leqslant O(10^{-2})$. The observed B^0–$\widetilde{B}^0$ mixing implies that $\Delta m_B/\Gamma_B=0.74\pm0.04$, which means that $|\Delta\Gamma_B|\ll\Delta m_B$. Therefore, the lifetime difference between the CP eigenstates is very small, and it is possible to define these states as "light" and "heavy": $B_L=B_1$ and $B_H=B_2$. It follows that $|\Gamma_{12}|\ll|M_{12}|$, and to first order in Γ_{12}/M_{12} we find

$$\left|\frac{q}{p}\right|_B-1\simeq-2\,\mathrm{Re}(\widetilde{\epsilon}_B)=O(10^{-2}). \tag{123}$$

Since B_L and B_H have almost identical lifetimes, it is not possible to produce selectively beams of B_L and B_H particles. The time evolution of an initially pure B^0 state is

$$|B^0(t)\rangle=e^{-im_Bt}e^{-1/2\Gamma_Bt}\left(\cos\left(\frac{1}{2}\Delta m_Bt\right)|B^0\rangle+\frac{iq}{p}\sin\left(\frac{1}{2}\Delta m_Bt\right)|\widetilde{B}^0\rangle\right), \tag{124}$$

$$|\widetilde{B}^0(t)\rangle=e^{-im_Bt}e^{-1/2\Gamma_Bt}\left(\cos\left(\frac{1}{2}\Delta m_Bt\right)|\widetilde{B}^0\rangle+\frac{ip}{q}\sin\left(\frac{1}{2}\Delta m_Bt\right)|B^0\rangle\right), \tag{125}$$

where $m_{H,L}=m_B\pm1/2\Delta m_B$, and $\Gamma_{H,L}\simeq\Gamma_B$. Defining the semileptonic asymmetry as

$$a_{SL}^B=\frac{\Gamma(\widetilde{B}^0(t)\to l^+\bar{\nu}X)-\Gamma(B^0(t)\to l^-\nu X)}{\Gamma(\widetilde{B}^0(t)\to l^+\bar{\nu}X)+\Gamma(B^0(t)\to l^-\nu X)}, \tag{126}$$

we find

$$a_{SL}^B=\frac{1-|q/p|^4}{1+|q/p|^4}\simeq4\,\mathrm{Re}(\widetilde{\epsilon}_B)=O(10^{-2}). \tag{127}$$

At present, we have no experimental evidence for indirect CP violation in the B-meson system.

Consider decays of neutral mesons into CP eigenstates:

$$A=\langle f_{CP}|H|P^0\rangle,\quad A^*=\langle f_{CP}|H|\widetilde{P}^0\rangle. \tag{128}$$

The condition $\lambda=(q/p)\cdot(\bar{A}/A)\neq1$ implies CP violation. The most theoretically favored scenario is when $\lambda=e^{i\phi\lambda}$. In that case λ is a pure phase, and the hadronic uncertainties cancel. We define the CP asymmetry as

$$a_{f_{CP}}=\frac{\Gamma(B^0(t)\to f_{CP})-\Gamma(\widetilde{B}^0(t)\to f_{CP})}{\Gamma(B^0(t)\to f_{CP})+\Gamma(\widetilde{B}^0(t)\to f_{CP})}. \tag{129}$$

Since $|q/p|_B \simeq 1$, we find

$$a_{f_{CP}} \simeq \frac{(1-|\lambda|^2)\cos(\Delta m_B t) - 2Im\lambda \sin(\Delta m_B t)}{1+|\lambda|^2}. \quad (130)$$

Decays of neutral B mesons into CP eigenstates provide a model-independent determination of the CP-violating phase. In the B-meson system we have

$$\left(\frac{q}{p}\right)_B \simeq -\frac{M_{12}^*}{|M_{12}|} = \frac{(V_{tb}^* V_{td})^2}{|V_{tb}^* V_{td}|^2} = \frac{V_{tb}^* V_{td}}{V_{tb} V_{td}^*} = e^{-2i\beta}. \quad (131)$$

To eliminate the hadronic uncertainties, it is necessary to choose decay modes which are dominated by a single diagram. Examples of such decays are $\tilde{B} \to \pi\pi$, $\tilde{B} \to D\bar{D}$, $B_s \to \phi K_S$, $\tilde{B} \to \rho K_S$, $B_S \to \psi K_S$, $\tilde{B} \to \phi K_S$, $\tilde{B} \to K_S K_S$, $B_s \to \eta'\eta'$, $B_s \to \phi K_S$, and $B_s \to \psi\phi$

Tree-dominated decays: $\tilde{B} \to \pi\pi$. The decay $\tilde{B} \to \pi\pi$ proceeds through the quark decay $b \to u\bar{u}d$, for which the tree and the penguin diagrams have CKM parameters of order λ^3. Thus, the tree diagram is dominant, and

$$\lambda_{\pi\pi} = \frac{q}{p} \cdot \frac{\tilde{A}}{A} \simeq \frac{V_{tb}^* V_{td}}{V_{tb} V_{td}^*} \cdot \frac{V_{ub} V_{ud}^*}{V_{ub}^* V_{ud}} = e^{-2i\beta} e^{-2i\gamma} = e^{2i\alpha}, \quad (132)$$

$$\mathrm{Im}(\lambda_{\pi\pi}) \simeq \sin(2\alpha). \quad (133)$$

Hadronic uncertainties arise from the small admixture of penguin contributions, and they are expected to be of order 10%.

Tree-forbidden decays: $\tilde{B} \to \phi K_S$. The decay $\tilde{B} \to \phi K_S$ proceeds through the quark transition $b \to s\bar{s}s$, i.e., it is forbidden at the tree level, and only the penguin diagram contributes. A new ingredient here is the presence of $K-\bar{K}$ mixing, which adds a factor

$$\left(\frac{q}{p}\right)_K \simeq \frac{V_{cs} V_{cd}^*}{V_{cs}^* V_{cd}} \quad (134)$$

in the definition of λ. We find

$$\lambda_{\phi K_S} = \left(\frac{q}{p}\right)_B \cdot \left(\frac{q}{p}\right)_K \cdot \frac{\tilde{A}}{A} \simeq \frac{V_{tb}^* V_{td}}{V_{tb} V_{td}^*} \cdot \frac{V_{cs} V_{cd}^*}{V_{cs}^* V_{cd}} \cdot \frac{V_{tb} V_{ts}^*}{V_{tb}^* V_{ts}} = e^{-2i\beta}, \quad (135)$$

$$\mathrm{Im}(\lambda_{\phi K_S}) \simeq -\sin(2\beta). \quad (136)$$

Decays with a single weak phase: $\tilde{B} \to \psi K_S$. The decay $\tilde{B} \to \psi K_S$ is based on the quark transition $b \to c\bar{c}s$, for which the tree diagram is dominant. We find

$$\lambda_{\psi K_S} = -\left(\frac{q}{p}\right)_B \cdot \left(\frac{q}{p}\right)_K \cdot \frac{\tilde{A}}{A} \simeq -e^{-2i\beta}, \quad (137)$$

$$\mathrm{Im}(\lambda_{\psi K_S}) \simeq \sin(2\beta). \quad (138)$$

The hadronic uncertainties for this decay are of order 10^{-3}.

Note that the angle β', which appears in the CP asymmetries for B_s-meson decay, is the analog of the angle β in the unitarity triangle defined by the relation

$$V_{us} V_{ub}^* + V_{cs} V_{cb}^* + V_{ts} V_{tb}^* = 0. \quad (139)$$

Experimentally, $|\sin(2\beta')| \leq 0.06$.

3.2.5. B physics at CMS

Three experiments are foreseen for the B-physics investigation at LHC. ATLAS, and CMS are two general-purpose experiments designed to look for the Higgs boson and supersymmetric particles. LHC-B[26] is a dedicated experiment to study CP violation. Since ATLAS and CMS are designed to look for particles produced in a very hard collision, the detectors cover the central region. For the initial phase of the LHC operation, in which the luminosity is about 10^{33} cm^{-2} s^{-1}, it is intended to do physics with B mesons. The b-quark events are triggered by the high-transverse-momentum (p_t) lepton trigger by reducing the threshold value.

In LHC-B the forward geometry was chosen for the following reasons:[27]

1. The b-quark production is peaked in the forward direction, and in the forward region both b and $\bar{b}$ go in the same direction. Therefore, a single-arm spectrometer, with a modest angular coverage of up to $\sim$400 mrad, can detect 10–20% of the $b\bar{b}$ events, for which the decay products of the two b hadrons are within the detector acceptance. This reduces the cost of the detector.

2. B hadrons produced in the forward direction are faster than those in the central region. Their average momentum is about 80 GeV, corresponding to a mean decay length of $\sim$7 mm. Therefore, a good decay-time resolution can be obtained for reconstructed B mesons.

3. In the forward region, the momenta are carried mainly by the longitudinal components. Therefore, the threshold value for the p_t trigger can be set low for electrons, muons, and hadrons at about 1.5 GeV. This makes the p_t trigger more efficient than in the central region.

4. The detector can be built in an open geometry, which allows easy installation and maintenance.

5. LHC-B is the only detector capable of separating kaons from pions in all the necessary phase space.

Here we briefly describe the B-physics potential of CMS. The ATLAS B-physics potential is similar. As has been mentioned before, the main CP-violation prediction for B systems is the inequality $\Gamma(B^0 \to f) \neq \Gamma(\bar{B}^0 \to \bar{f})$. The decay-rate asymmetry

$$A = \frac{\Gamma(B^0 \to f) - g\Gamma(\bar{B}^0 \to \bar{f})}{\Gamma(B^0 \to f) + \Gamma(\bar{B}^0 \to \bar{f})} \sim \sin(2\Phi) \quad (140)$$

depends only on the CP-violating angles of the triangle, $\alpha, \gamma, \beta = \Phi$. At LHC the cross section for $pp \to b\bar{b} + \ldots$ is expected to be in the range 0.08–0.6 mb. The most promising channels for the search for CP violation are $B_d^0 \to (\psi \to \mu^+\mu^-) + (K_s^0 \to \pi^+\pi^-)$ and $B_d^0 \to \pi^+\pi^-$.

The decay $B_d^0 \to \psi K_S^0$ with $\psi \to \mu^+\mu^-$ and $K_S^0 \to \pi^+\pi^-$ is the most appropriate channel to measure the angle β. To tag the B_d^0, the associated b hadron is required to decay into a muon $+X$. The time-integrated asymmetry A is

$$A = \frac{N^+ - N^-}{N^+ + N^-} = D \cdot \frac{x_d}{1+x_d^2} \cdot \sin(2\beta), \quad (141)$$

where N^+ and N^- are the numbers of events with positively and negatively charged tagging muons, D is the dilution factor, and $x_d/(1+x_d^2)$ is the time-integration factor. The expected number of events for an integrated luminosity L is

$$N=2\times L\times\sigma_{b\bar{b}}\times P(\bar{b}\to B_d^0)\times \mathrm{Br}(B_d^0\to\psi K_S^0)\times \mathrm{Br}(\psi \to\mu^+\mu^-)\times \mathrm{Br}(K_S^0\to\pi^+\pi^-)\times \mathrm{Br}(b\to\mu)\times A_{\mathrm{trig}}\times\epsilon, \tag{142}$$

where A_{trig} is the trigger acceptance, and ε is the efficiency of the selection cuts. Typical values of the branching ratios are: $P(\bar{b}\to B_d^0)=0.4$; $\mathrm{Br}(B_d^0\to\psi K_S^0)=3.3\times10^{-4}$; $\mathrm{Br}(\psi\to\mu^+\mu^-)=0.0597$; $\mathrm{Br}(K_S^0\to\pi^+\pi^-)=0.6861$; $\mathrm{Br}(b\to\mu)=0.105$. Before trigger-acceptance and data-selection cuts, the number of produced signal events is 5.6×10^6 for 10^4 pb^{-1}. The measured asymmetry A is affected by dilution factors $D\simeq0.47$. The signal-to-background ratio is estimated to be $S/b\approx10:1$, and the mixing angle $\sin(2\beta)$ is determined with accuracy ≈0.05 for $L_t=10^4$ pb^{-1}.

The $B_d^0\to\pi^+\pi^-$ decay is a good channel to determine the angle α of the unitarity triangle. For $L_t=10^4$ pb^{-1} the sensitivity to the determination of the angle α of the triangle is estimated to be $\delta(\sin(2\alpha))=0.057\pm0.018$.

CP violation in B_d^0 and $\bar{B}_d^0$ decays gives rise to different decay rates with a time dependence. The asymmetry can be measured as a function of the proper time t/τ in units of the B_d^0 lifetime τ:

$$A(t/\tau)=\frac{N^--N^+}{N^-+N^+}=D\cdot\eta_{CP}\cdot\sin(2\varphi_i)\cdot\sin(x_dt/\tau), \tag{143}$$

where N^+ and N^- are the numbers of events with positively and negatively charged tagging muons, D is the dilution factor, η_{CP} is the CP parity of the final state f, and φ_i is the angle of the unitarity triangle. It is possible to measure the secondary vertex in the transverse plane to determine the time-dependent asymmetry and hence to determine the CP-violating angles α and β.[1] The accuracy in the determination of the angles α and β is similar to the accuracy for the case of the time-integrated asymmetry considered previously.

A very important task of B physics at LHC is the observation of $B_s^0-\bar{B}_s^0$ oscillations, but this could be very difficult if x_s is large. The current limits on the value of x_s are $5.6\leqslant x_s\leqslant33.2$ (Ref. 28). The possibility of discovering $B_s^0-\bar{B}_s^0$ oscillations at LHC was studied in Ref. 29.

Another interesting task is the search for the rare decay $B_s^0\to\mu^+\mu^-$. This decay is forbidden at the tree level. In the standard model the branching ratio of this decay is expected to be $\approx2\times10^{-9}$ (Ref. 30). It appears that at CMS the upper limit on this branching ratio can be set at 1.4×10^{-9} at a 90% C.L. for $L_t=3\times10^4$ pb^{-1} (Ref. 1).

3.2.6. Heavy-ion physics

Quantum chromodynamics has already proved itself to be a reliable theory when dealing with quark and gluon interactions at short distances. The QCD vacuum exhibits properties similar to those of a superconductor. It has a critical temperature beyond which it becomes transparent to color. This temperature is found to be of the order of 150–200 MeV.[31] Consider a system consisting of a set of hadrons in the vacuum, and compress it. The hadrons are initially too far apart to overlap. As the density increases, they start overlapping among themselves. We thus go from a dilute to a very dense hadron gas. With increasing compression, the hadrons merge with each other. The small vacuum bubbles separately associated with each individual hadron should eventually fuse into one big bubble within which quarks move freely over distances much larger than those offered by the hadrons in which they were first confined. Since in high-energy collisions new particles are created out of the collision energy, we reach the same conclusions if the initial dilute hadron gas is heated instead of being merely compressed. In heavy-ion collisions we have a complicated mixture of compression and heating. Computer calculations support the naive picture, according to which at low temperature we have a hadron gas, while at high temperature we have a quark–gluon plasma.[31] Naively, we can expect the following picture in heavy-ion collisions at high energies:[31]

1. An initial phase during which many collisions occur at the parton level. A large number of energetic partons are formed. The system is still far from any equilibrium. A large amount of entropy is released.

2. A thermalized phase, obtained through the scattering of the many partons. The temperature is very high. The system is a quark–gluon plasma, at least in some localized regions.

3. A mixed phase, obtained as the plasma cools, with parts of it hadronizing as the temperature goes through its critical value.

4. A thermalized, dense hadron gas from which hadrons eventually escape as their mean free path exceeds the size of the system. This is what is referred to as freeze-out.

However, all the processes occur in a very short time. When we look at the dominantly produced hadrons, we merely integrate over the whole evolution. Thus, any evidence for a quark–gluon plasma is averaged over the past history. In other words, after the transition from quark–gluon plasma to the hadron phase the system can "forget" about the previous phase. The most striking signal associated with quark–gluon plasma is the suppression of charmonium and upsilonium formation.[32]

The physical picture leading to ψ suppression due to quark deconfinement in nuclear collisions is quite simple. Within a deconfining medium like QGP (quark–gluon plasma), quarks cannot bind to form hadrons. The heavy charm quark–antiquark pairs which form ψ are produced by hard, prethermal interactions at a very early stage of the collision. In a deconfining medium, c and $\bar{c}$ just fly apart. Moreover, within the equilibrated QGP the production of additional thermal c quarks is strongly suppressed by a factor $\exp(-m_c/T_c)\simeq0.6\times10^{-3}$ with a charmed-quark mass $m_c=1.5$ GeV and $T_c=0.2$ GeV. Consequently, ψ production will be suppressed in the presence of QGP. In atomic physics, the screened binding potential between two charges is given by $V=V_0\exp(-r/r_D)$, where r_D is the Debye radius. When $r_D\approx r_B$, the valence electrons are liberated, because

of charge screening, and the insulator changes into a conductor. Similarly, in QCD the potential between two colored quarks is given by $V=V_0\exp(-r/r_D)$ because of color screening, and if the density of color charges is sufficient to make $r_D \leqslant r_H$ (the hadron radius), the color insulators of hadrons change into a color-conducting phase, i.e., QGP. This means that the long-range confining phase of the potential becomes screened, i.e., we have quark deconfinement. We need to know the ψ radius and the screening radius r_D at a given temperature. Only for $r_D \leqslant r_\psi$ can we expect ψ suppression. It has been found[31] that $r_D=r_H$ occurs near the transition temperature T_c for ψ', and $T/T_c \geqslant 1.3$ for ψ. Recent NA50 data[33] support this picture. It should be noted, however, that ψ suppression can also be explained either on the basis of absorption processes in a dense hadron gas or on the basis of conventional nuclear effects.[34] For LHC energies with the center-of-mass energy about 6 TeV per nucleon and with the energy density $\epsilon \approx 9$ GeV/fm^3, all the heavy-quark bound states except $\Upsilon(1S)$ will be suppressed by color screening.

The main goal of the LHC heavy-ion program is the search for quark–gluon plasma. There will be a special detector ALICE[35] dedicated to the heavy-ion investigation at LHC. Here we briefly describe the "heavy-ion potential" of CMS.[1] The most promising signature here is a measurement of the production rates of the bottomonium states for different nuclei and different kinematics. The most interesting signature is the measurement of the cross section of the Υ state as a function of p_T^{Υ}, since no suppression due to Debye color screening is expected.[31,32]. As has been mentioned before, a typical prediction of the existence of quark–gluon plasma in this case is the suppression of $\Upsilon(2S)$ and $\Upsilon(3S)$ relative to the $\Upsilon(1S)$ yield. Simulation studies were performed for ^{16}O, ^{40}Ca, ^{97}Nb, and ^{208}Pb ion collisions. The ψ and Υ resonances were generated by using p_t and y distributions extrapolated from experimental results obtained at lower $\sqrt{s}$. The total acceptance for $\Upsilon \to \mu\mu$ was found to be ≈ 0.33, and for ψ it is around 0.06. If we restrict the analysis to the barrel region, where muons with $p_t \geqslant 4$ GeV can be detected, the acceptance for Υ decreases to 0.05, and for ψ it vanishes. It was found that the mass resolution for Υ is about 40 MeV. The cross sections for Υ production in $A-A$ collisions were obtained by multiplying the cross sections for the pp reaction at the same c.m.s. energy by a factor $A^{2\alpha}$ with $\alpha=0.95$. The main dimuon background is due to uncorrelated muon pairs from π and K decays. The signal-to-background ratios have been calculated in the mass band $M(\Upsilon)\pm 50$ MeV, for central collisions of Pb, Ca, Nb, and O beams. The results depend rather strongly on the value of $\sigma(pp\to\Upsilon)$ and on the charged-particle multiplicity $dn^{\pm}/dy$ per unit rapidity in the central collisions. The main conclusion from these studies is that CMS will be capable of detecting Υ, Υ', and Υ'' resonances reliably.

Another interesting prediction, testable at CMS, is jet quenching in quark–gluon plasma. As jets are produced early in a collision, they propagate in the plasma, and interact strongly before they escape. Hence, they carry information about deconfined hadronic matter. The problems of finding jets at CMS with large transverse-energy (E_t) flow in central collisions were studied, to determine the possibilities of observing jet quenching using CMS.[36] The high-E_t jet-production cross section in Pb–Pb collisions was estimated in the rapidity region $|y| \leqslant 1.5$, using the jet cross section for pp interactions, as evaluated by PYTHIA, and an $A^{2\alpha}$ dependence for the $A-A$ collisions. The effect of energy losses in dense nuclear matter, changing the high-E_t jet-production cross section, was disregarded. A central event with two high-E_t jets from a proton–proton collision was superimposed on the ion collision. The main conclusion from these studies is that jets can be reliably reconstructed in the CMS detector for Pb–Pb central collisions with $E_t \geqslant 100$ GeV.[36]

3.3. Supersymmetry search within the MSSM

3.3.1. The MSSM model

Supersymmetry (SUSY) is a new type of symmetry that relates the properties of bosons to those of fermions.[37] It is the largest symmetry of the S matrix. Locally, supersymmetric theories necessarily incorporate gravity.[38] SUSY is also an essential ingredient of superstring theories.[39] The recent interest in supersymmetry is due to the observation that measurements of the gauge coupling constants at LEP1 favor grand unification in a supersymmetric theory with superpartners of ordinary particles which are lighter than $O(1)$ TeV. Supersymmetric electroweak models also offer the simplest solution of the gauge hierarchy problem.[37] In real life, supersymmetry must be broken, and to solve the gauge hierarchy problem the masses of superparticles must be lighter than $O(1)$ TeV. Supergravity gives a natural explanation of supersymmetry breaking,[38] namely, allowance for supergravity breaking in the hidden sector leads to soft supersymmetry breaking in the observable sector. The simplest supersymmetric generalization of the standard model is the Minimal Supersymmetric Standard Model (MSSM). It is a supersymmetric theory based on the standard $SU_c(3)\otimes SU_L(2)\otimes U(1)$ gauge group with electroweak symmetry spontaneously broken via vacuum expectation values of two different Higgs doublets. The MSSM consists of taking the standard model and adding the corresponding supersymmetric partners. It should be stressed that in addition the MSSM contains two hypercharge $Y=\pm 1$ Higgs doublets, which is the minimal structure for the Higgs sector of an anomaly-free supersymmetric extension of the standard model. The supersymmetric electroweak models also require at least two Higgs doublets to generate masses for both "up"-type and "down"-type fermions. The renormalizable superpotential determines the Yukawa interactions of quarks and leptons, and it preserves global $B-L$. Here B is the baryon number, and L is the lepton number. Note that the most general expression for the effective superpotential contains renormalizable terms violating $B-L$, which can lead to problems with proton decay. To eliminate such dangerous terms in the superpotential, R-parity conservation of the theory is postulated. Here $R=(-1)^{3(B-L)+2S}$ for a particle of spin S. This formula means that all ordinary standard-model particles have $R=1$, whereas the corresponding supersymmetric partners have $R=-1$. The R-parity conservation has a crucial impact on supersymmetric phenomenology. An important

consequence of R-parity conservation is that the lightest supersymmetric particle (LSP) is stable. Cosmological constraints imply that the LSP is a weakly interacting, electrically neutral, and colorless particle. Another important consequence of R-parity conservation is that at supercolliders the superparticles must be produced in pairs, and therefore at least two LSPs must eventually be produced at the end of the decays of heavy, unstable, supersymmetric particles. Being a weakly interacting particle, the LSP escapes detector registration, and therefore the classic signature for R-parity conserving supersymmetric theories is the transverse missing energy due to the LSP escape. Note that at present, there are no deep theoretical arguments in favor of R-parity conservation. There are models with R-parity violation.[40] Models with R-parity violation break the $B-L$ number and are strongly constrained by existing experimental data. In such models the LSP is unstable, supersymmetric particles can be singly produced, and, in general, the signature related to the transverse missing energy is lost.

The superpotential of the MSSM is

$$W=h^u_{ij}U^c_i Q_j H_2+h^d_{ij}D^c_i Q_j H_1+h^l_{ij}E^c_i L_j H_1-\mu H_1 H_2, \tag{144}$$

where i and j are summed over 1,2,3; Q_j, U^c_a, and D^c_b denote the $SU(2)$ doublet and $SU(2)$ singlet quark superfields, L^i, and E^c_i are the $SU(2)$ doublet and $SU(2)$ singlet lepton superfields, H_1, and H_2 denote the two Higgs superdoublets, and h^u_{ij}, h^d_{ij}, and h^l_{ij} are the Yukawa coupling constants. In the MSSM, supersymmetry is softly broken at some high scale M by generic soft terms

$$\begin{aligned}-L_{\text{soft}}=&m_0(A^u_{ij}U^c_i Q_j H_2+A^d_{ij}D^c_i G_j H_1+A^l_{ij}E^c_i L_j H_1\\&+\text{H.c.})+(m^2_q)_{ij}Q^+_i Q_j+(m^2_u)_{ij}(U^c_i)^+U^c_j\\&+(m^2_d)_{ij}(D^c_i)^+D^c_j+(m^2_l)_{ij}(L^c_i)^+L^c_j\\&+(m^2_e)_{ij}(E^c_i)^+E^c_j+m^2_1 H_1 H^+_1+m^2_2 H_2 H^+_2\\&+(Bm^2_0 H_1 H_2+\text{H.c.})+\frac{1}{2}m_a(\lambda_a\lambda_a).\end{aligned} \tag{145}$$

In most analyses the mass terms are assumed to be diagonal at the $M_{\text{GUT}}\approx 2\times 10^{16}$ GeV scale, and the gaugino and trilinear mass terms are assumed to be universal at the M_{GUT} scale, i.e., at the GUT scale

$$\begin{aligned}&A^u_{ij}(M_{\text{GUT}})=Ah^u_{ij}(M_{\text{GUT}}),\\&A^d_{ij}(M_{\text{GUT}})=Ah^d_{ij}(M_{\text{GUT}}),\quad A^l_{ij}(M_{\text{GUT}})=Ah^l_{ij}(M_{\text{GUT}}),\end{aligned} \tag{146}$$

$$\begin{aligned}(m^2_q)_{ij}(M_{\text{GUT}})&=(m^2_u)_{ij}(M_{\text{GUT}})=(m^2_d)_{ij}(M_{\text{GUT}})\\&=(m^2_l)_{ij}(M_{\text{GUT}})=(m^2_e)_{ij}(M_{\text{GUT}})\\&=\delta_{ij}m^2_1(M_{\text{GUT}})=\delta_{ij}m^2_2(M_{\text{GUT}})=\delta_{ij}m^2_0,\end{aligned} \tag{147}$$

$$m_1(M_{\text{GUT}})=m_2(M_{\text{GUT}})=m_3(M_{\text{GUT}})=m_{1/2}. \tag{148}$$

Note that it is more appropriate to impose boundary conditions not at the GUT scale, but at the Planck scale, $M_{\text{Pl}}=2.4\times 10^{18}$ GeV. Allowance for renormalization effects between the Planck scale and the GUT scale can drastically change the features of the spectrum. For instance, if we assume that the physics between the Planck scale and the GUT scale is described by the SUSY $SU(5)$ model, then allowance for the evolution between the Planck and GUT scales[41,42] changes qualitatively the spectrum of sleptons for $m_0 \ll m_{1/2}$.[42] Thus, in the MSSM we have unknown soft supersymmetry-breaking parameters $m_0, m_{1/2}, A$, and B, and we also have an unknown parameter μ in the superpotential. The renormalization-group equations for the soft SUSY-breaking parameters, without allowance for all the Yukawa coupling constants except the top-quark Yukawa constant in the one-loop approximation, are[43]

$$\frac{d\tilde{m}^2_L}{dt}=\left(3\tilde{\alpha}_2 M^2_2+\frac{3}{5}\tilde{\alpha}_1 M^2_1\right), \tag{149}$$

$$\frac{d\tilde{m}^2_E}{dt}=\left(\frac{12}{5}\tilde{\alpha}_1 M^2_1\right), \tag{150}$$

$$\begin{aligned}\frac{d\tilde{m}^2_Q}{dt}=&\left(\frac{16}{3}\tilde{\alpha}_3 M^2_3+3\tilde{\alpha}_2 M^2_2+\frac{1}{15}\tilde{\alpha}_1 M^2_1\right)-\delta_{i3}Y_t(\tilde{m}^2_Q\\&+\tilde{m}^2_U+m^2_2+A^2_t m^2_0-\mu^2),\end{aligned} \tag{151}$$

$$\begin{aligned}\frac{d\tilde{m}^2_U}{dt}=&\left(\frac{16}{3}\tilde{\alpha}_3 M^2_3+\frac{16}{15}\tilde{\alpha}_1 M^2_1\right)-\delta_{i3}2Y_t(\tilde{m}^2_Q+\tilde{m}^2_U+m^2_2\\&+A^2_t m^2_0-\mu^2),\end{aligned} \tag{152}$$

$$\frac{d\tilde{m}^2_D}{dt}=\left(\frac{16}{3}\tilde{\alpha}_3 M^2_3+\frac{4}{15}\tilde{\alpha}_1 M^2_1\right), \tag{153}$$

$$\frac{d\mu^2}{dt}=3\left(\tilde{\alpha}_2+\frac{1}{5}\tilde{\alpha}_1-Y_t\right)\mu^2, \tag{154}$$

$$\frac{dm^2_1}{dt}=3\left(\tilde{\alpha}_2 M^2_2+\frac{1}{5}\tilde{\alpha}_1 M^2_1\right)+3\left(\tilde{\alpha}_2+\frac{1}{5}\tilde{\alpha}_1-Y_t\right)\mu^2, \tag{155}$$

$$\begin{aligned}\frac{dm^2_2}{dt}=&3\left(\tilde{\alpha}_2 M^2_2+\frac{1}{5}\tilde{\alpha}_1 M^2_1\right)+3\left(\tilde{\alpha}_2+\frac{1}{5}\tilde{\alpha}_1\right)\mu^2\\&-3Y_t(\tilde{m}^2_Q+\tilde{m}^2_U+m^2_2+A^2_t m^2_0),\end{aligned} \tag{156}$$

$$\begin{aligned}\frac{dA_t}{dt}=&-\left(\frac{16}{3}\tilde{\alpha}_3\frac{M_3}{m_0}+3\tilde{\alpha}_2\frac{M_2}{m_0}+\frac{13}{15}\tilde{\alpha}_1\frac{M_1}{m_0}\right)\\&-6Y_t A_t,\end{aligned} \tag{157}$$

$$\frac{dB}{dt}=-3\left(\tilde{\alpha}_2\frac{M_2}{m_0}+\frac{1}{5}\tilde{\alpha}_1\frac{M_1}{m_0}\right)-3Y_t A_t, \tag{158}$$

$$\frac{dM_i}{dt}=-b_i\tilde{\alpha}_i M_i, \tag{159}$$

$$b_1=\frac{33}{5},\quad b_2=1,\quad b_3=-3. \tag{160}$$

Here $\tilde{m}_U, \tilde{m}_D$, and $\tilde{m}_E$ refer to the masses of the superpartners of the quark and lepton singlets, and $\tilde{m}_Q$ and $\tilde{m}_L$ refer to the masses of the isodoublet partners; m_1, m_2, m_3, and μ are the mass partners of the Higgs potential; A and B are the

couplings of L_{soft}, as defined before; and M_i are the gaugino masses before mixing. The renormalization-group equation for the top Yukawa coupling constant is

$$\frac{dY_t}{dt}=Y_t\left(\frac{16}{3}\,\tilde{\alpha}_3+3\tilde{\alpha}_2+\frac{13}{15}\,\tilde{\alpha}_1\right)-6Y_t^2, \tag{161}$$

while the renormalization-group equations for the gauge couplings are

$$\frac{d\tilde{\alpha}_i}{dt}=-b_i\tilde{\alpha}_i^2. \tag{162}$$

Here

$$\tilde{\alpha}_i=\frac{\alpha_i}{4\pi},\quad Y_t=\frac{h_t^2}{16\pi^2},\quad t=\ln\left(\frac{M_{\text{GUT}}^2}{Q^2}\right), \tag{163}$$

and the top Yukawa coupling h_t is related to the running top mass by the equation

$$m_t=h_t(m_t)\,\frac{v}{\sqrt{2}}\sin\beta. \tag{164}$$

The boundary conditions at $Q^2=M_{\text{GUT}}^2$ are

$$\tilde{m}_Q^2=\tilde{m}_U^2=\tilde{m}_D^2=\tilde{m}_E^2=\tilde{m}_L^2=m_0^2, \tag{165}$$

$$\mu=\mu_0;\quad m_1^2=m_2^2=\mu_0^2+m_0^2;\quad m_3^2=B\mu_0 m_0, \tag{166}$$

$$M_i=m_{1/2},\quad \tilde{\alpha}_i(0)=\tilde{\alpha}_{\text{GUT}};\quad i=1,2,3. \tag{167}$$

For the gauginos of the $SU(2)\otimes U(1)$ gauge group one must consider the mixings with the Higgsinos. The mass terms in the full Lagrangian are[44]

$$L_{\text{Gaugino-Higgsino}}=-\frac{1}{2}\,M_3\bar{\lambda}_3^a\lambda_3^a-\frac{1}{2}\,\bar{\chi}M^{(0)}\chi-(\bar{\psi}M^{(c)}\psi+\text{H.c.}), \tag{168}$$

where λ_3^a are the eight Majorana gluino fields, and

$$\chi=\begin{pmatrix}\tilde{B}^0\\ \tilde{W}^3\\ \tilde{H}_1^0\\ \tilde{H}_2^0\end{pmatrix}, \tag{169}$$

$$\psi=\begin{pmatrix}\tilde{W}^+\\ \tilde{H}^+\end{pmatrix} \tag{170}$$

are the Majorano neutralino and Dirac chargino fields. The mass matrices are

$$M^{(0)}=\begin{pmatrix}M_1 & 0 & -A & B\\ 0 & M_2 & C & -D\\ -A & C & 0 & -\mu\\ B & -D & -\mu & 0\end{pmatrix}, \tag{171}$$

$$M^{(c)}=\begin{pmatrix}M_2 & \sqrt{2}M_W\sin\beta\\ \sqrt{2}M_W\cos\beta & \mu\end{pmatrix}, \tag{172}$$

where

$$A=M_Z\cos\beta\sin\theta_W,\quad B=M_Z\sin\beta\sin\theta_W, \tag{173}$$

$$C=M_Z\cos\beta\cos\theta_W,\quad D=M_Z\sin\beta\cos\theta_W. \tag{174}$$

After the solution of the corresponding renormalization-group equations for $\alpha_{\text{GUT}}=1/24.3$, $M_{\text{GUT}}=2.0\times10^{16}$ GeV, $\sin^2\theta_W=0.2324$, and $A_t(0)=0$, we find the following numerical formulas for the squark and slepton squared masses:[45]

$$\tilde{m}_{E_L}^2(t=66)=m_0^2+0.52m_{1/2}^2-0.27\cos2\beta M_Z^2, \tag{175}$$

$$\tilde{m}_{\nu_L}^2(t=66)=m_0^2+0.52m_{1/2}^2+0.5\cos2\beta M_Z^2, \tag{176}$$

$$\tilde{m}_{E_R}^2(t=66)=m_0^2+0.15m_{1/2}^2-0.23\cos2\beta M_Z^2, \tag{177}$$

$$\tilde{m}_{U_L}^2(t=66)=m_0^2+6.5m_{1/2}^2+0.35\cos2\beta M_Z^2, \tag{178}$$

$$\tilde{m}_{D_L}^2(t=66)=m_0^2+6.5m_{1/2}^2-0.42\cos2\beta M_Z^2, \tag{179}$$

$$\tilde{m}_{U_R}^2(t=66)=m_0^2+6.1m_{1/2}^2+0.15\cos2\beta M_Z^2, \tag{180}$$

$$\tilde{m}_{D_R}^2(t=66)=m_0^2+6.0m_{1/2}^2-0.07\cos2\beta M_Z^2, \tag{181}$$

$$\tilde{m}_{b_R}^2(t=66)=\tilde{m}_{D_R}^2, \tag{182}$$

$$\tilde{m}_{b_L}^2(t=66)=\tilde{m}_{D_L}^2-0.49m_0^2-1.21m_{1/2}^2, \tag{183}$$

$$\tilde{m}_{t_R}^2(t=66)=\tilde{m}_{t_R}^2(t=66)=\tilde{m}_{U_R}^2(t=66)+m_t^2-0.99m_0^2-2.42m_{1/2}^2, \tag{184}$$

$$\tilde{m}_{t_L}^2(t=66)=\tilde{m}_{U_L}^2(t=66)+m_t^2-0.49m_0^2-1.21m_{1/2}^2. \tag{185}$$

After mixing, the mass eigenstates of the stop matrix are

$$\tilde{m}_{t_{1,2}}^2(t=66)\approx\frac{1}{2}\,[0.5m_0^2+9.1m_{1/2}^2+2m_t^2+0.5\cos2\beta M_Z^2]\mp\frac{1}{2}\,[(1.5m_{1/2}^2+0.5m_0^2+0.2\cos(2\beta)M_Z^2)^2+4m_t^2(A_tm_0-\mu/\tan\beta)^2]^{1/2}. \tag{186}$$

The gauginos and Higgsinos have similar quantum numbers, and this causes mixing between the weak-interaction eigenstates and the mass eigenstates. The two chargino eigenstates $\chi_{1,2}^{\pm}$ are

$$M_{1,2}^2=\frac{1}{2}\,[M_2^2+\mu^2+2M_W^2]\mp\frac{1}{2}\,[(M_2^2-\mu^2)^2+4M_W^4\cos^2 2\beta+4M_W^2(M_2^2+\mu^2+2M_2\mu\sin2\beta)]^{1/2}, \tag{187}$$

where at the GUT scale the masses of the gaugino fields of the $SU(3)$, $SU_L(2)$, and $U(1)$ groups are equal to $m_{1/2}$. The eigenvalues of the 4×4 neutralino mass matrix can be found by numerical diagonalization. If the parameter μ is much larger than M_1 and M_2, the mass eigenstates become

$$\chi_i^0=\left[\tilde{B},\tilde{W}_3,\frac{1}{\sqrt{2}}\,(\tilde{H}_1-\tilde{H}_2),\frac{1}{\sqrt{2}}\,(\tilde{H}_1+\tilde{H}_2)\right], \tag{188}$$

with eigenvalues $|M_1|$, $|M_2|$, $|\mu|$, and $|\mu|$, respectively (the bino and neutral wino do not mix with each other, or with the Higgsino eigenstates).

The tree-level Higgs potential in the MSSM has the form

$$V_0(H_1,H_2)=m_1^2|H_1|^2+m_2^2|H_2|^2-m_3^2(H_1H_2+\text{H.c.}) + \frac{g_2^2+\tilde{g}_1^2}{8}(|H_1|^2-|H_2|^2)^2+\frac{g_2^2}{2}|H_1^+H_2|^2, \tag{189}$$

where $\tilde{g}_1^2=\frac{3}{5}g_1^2$.

Minimization of the effective potential $V_0(H_1,H_2)$ leads to the equations

$$v^2=\frac{8(m_1^2-m_2^2\tan^2\beta)}{(g_2^2+\tilde{g}_1^2)(\tan^2\beta-1)}, \tag{190}$$

$$\sin 2\beta=\frac{2m_3^2}{m_1^2+m_2^2}. \tag{191}$$

After diagonalization of the corresponding mass matrices, the CP-odd neutral Higgs boson $A(x)$ acquires a mass $m_A^2=m_1^2+m_2^2$, the charged Higgs boson $H^+(x)$ acquires a mass $m_{H^+}^2=m_A^2+M_W^2$, and the CP-even Higgs bosons $H(x)$ and $h(x)$ have masses

$$m_{H,h}^2=\frac{1}{2}[m_A^2+M_Z^2\pm\sqrt{(m_A^2+M_Z^2)^2-4m_A^2M_Z^2\cos^2 2\beta}], \tag{192}$$

where $\langle H_1\rangle=v_1=v\cos\beta/\sqrt{2}$, $\langle H_2\rangle=v_2=v\sin\beta/\sqrt{2}$, and $\tan\beta=v_2/v_1$. At the tree level we have the mass relations

$$m_h^2+m_H^2=m_A^2+M_Z^2, \tag{193}$$

$$m_h\leqslant m_A\leqslant m_H, \tag{194}$$

$$m_h\leqslant M_Z|\cos 2\beta|\leqslant M_Z. \tag{195}$$

Therefore, at the tree level the lightest Higgs boson is lighter than the Z boson. However, the radiative corrections due to the large top-quark Yukawa coupling constant increase the mass of the lightest Higgs boson in the MSSM.[46] The upper limit on the Higgs-boson mass in the MSSM depends on the values of the top-quark and stop-quark masses. For instance, for $m_t=175$ GeV and stop-quark masses lighter than 1 TeV it follows from Table I that the Higgs-boson mass must be lighter than 117 GeV. From the vacuum-stability bound ($k=0$ in Table I) we find that if the standard model is valid for energies up to 10^6 GeV, then the mass of the Higgs boson must exceed 121 GeV for $m_t=175$ GeV. Therefore, for $m_t=175$ GeV, we find that the Higgs-boson masses predicted for the SM and the MSSM lie in different mass intervals (in the MSSM the Higgs boson is relatively light, whereas in the SM it is relatively heavy). Thus, exact knowledge of the Higgs-boson mass would allow us to distinguish between the SM and the MSSM.[47] For instance, discovery of the Higgs boson at LEP2 would be very powerful evidence in favor of low-energy broken supersymmetry. After the solution of the corresponding equations for the determination of the nontrivial electroweak potential, the number of unknown parameters is decreased by two. At present, the more or less standard choice of the free parameters in the MSSM includes m_0, $m_{1/2}$, $\tan\beta$, A, and sign (μ).

Superparticle cross sections. At LHC sparticles can be produced via the following tree-level reactions:[48]

(i) $gg,qq,qg\to\tilde{g}\tilde{g},\tilde{g}\tilde{q},\tilde{q}\tilde{q}$;

(ii) $qq,gq\to\tilde{g}\tilde{\chi}_i^0,\tilde{g}\tilde{\chi}_i^\pm,\tilde{q}\tilde{\chi}_i^0,\tilde{q}\tilde{\chi}_i^\pm$;

(iii) $qq\to\tilde{\chi}_i^\pm\tilde{\chi}_j^\mp,\tilde{\chi}_i^\pm\tilde{\chi}_j^0,\tilde{\chi}_i^0\tilde{\chi}_j^0$;

(iv) $qq\to\tilde{l}\tilde{\nu}$, ll, $\tilde{\nu}\tilde{\nu}$.

The Higgs bosons of the MSSM can be produced via the direct s-channel subprocess:

(v) qq, $gg\to h$, H, A, $H^\pm H^\mp$.

It is straightforward to calculate the elementary (tree-level) cross sections for production of superparticles in collisions of quarks and gluons. Here, following Eichten *et al.*,[4] we collect the main formulas for the elementary cross sections.

The differential cross section for production of two gauge fermions in quark–antiquark collisions is

$$\frac{d\sigma}{dt}(q\bar{q}'\to\text{gaugino 1}+\text{gaugino 2}) = \frac{\pi}{s^2}\left[A_s\frac{(t-m_2^2)(t-m_1^2)+(u-m_1^2)(u-m_2^2)+2sm_1m_2}{(s-M_s^2)^2} + A_t\frac{(t-m_1^2)(t-m_2^2)}{(t-M_t^2)^2}+A_u\frac{(u-m_1^2)(u-m_2^2)}{(u-M_u^2)^2} + A_{st}\frac{(t-m_1^2)(t-m_2^2)+m_1m_2s}{(s-M_s^2)(t-M_t^2)} + A_{tu}\frac{m_1m_2s}{(t-M_t^2)(u-M_u^2)} + A_{su}\frac{(u-m_1^2)(u-m_2^2)+m_1m_2s}{(s-M_s^2)(u-M_u^2)}\right], \tag{196}$$

where m_1 and m_2 are the masses of the produced gauginos, and M_s, M_t, and M_u are the masses of the particles exchanged in the s, t, and u channels, respectively. The coefficients A_x are given in the paper of Eichten *et al.*[4] For instance, for the case of gluino pair production in quark–antiquark collisions the coefficients A_x are[47]

$$A_t=\tfrac{4}{9}A_s,\quad A_u=A_t,\quad A_{st}=A_s,\quad A_{su}=A_{st},$$

$$A_{tu}=\frac{1}{9}A_s,\quad A_s=\frac{8\alpha_s^2}{3}\delta_{qq'}.$$

The differential cross section for production of gluino pairs in gluon–gluon collisions is

$$\frac{d\sigma}{dt}(gg\to\tilde{g}\tilde{g})=\frac{9\pi\alpha_s^2}{4s^2}\left[\frac{2(t-m_{\tilde{g}}^2)(u-m_{\tilde{g}}^2)}{s^2} + \left[\left[\frac{(t-m_{\tilde{g}}^2)(u-m_{\tilde{g}}^2)-2m_{\tilde{g}}^2(t+m_{\tilde{g}}^2)0}{(t-m_{\tilde{g}}^2)^2} + \frac{(t-m_{\tilde{g}}^2)(u-m_{\tilde{g}}^2)+m_{\tilde{g}}^2(u-t)}{s(t-m_{\tilde{g}}^2)}\right]\right.\right.$$

$$+(t\leftrightarrow u)\left]\frac{m_{\tilde g}^2(s-4m_{\tilde g}^2)}{(t-m_{\tilde g}^2)(u-m_{\tilde g}^2)}\right]. \tag{197}$$

The total cross section is

$$\sigma(gg\to\tilde g\tilde g)=\frac{3\pi\alpha_s^2}{4s}\left[3\left[1+\frac{4m_{\tilde g}^2}{s}-\frac{4m_{\tilde g}^4}{s^2}\right]\ln\left[\frac{s+L}{s-L}\right]-\left[4+\frac{17m_{\tilde g}^2}{s}\right]\frac{L}{s}\right], \tag{198}$$

where $L=[s^2-4m_{\tilde g}^2 s]^{1/2}$.

The differential cross section for the reaction $q_iq_j\to\tilde q_i\tilde q_j$ in the case of equal masses of the right-handed and left-handed squarks is

$$\frac{d\sigma}{dt}(q_iq_j\to\tilde q_i\tilde q_j)=\frac{4\pi\alpha_s^2}{9s^2}\left[-\frac{(t-m_i^2)(t-m_j^2)+st}{(t-m_{\tilde g}^2)^2}-\delta_{ij}\frac{(u-m_i^2)(u-m_j^2)+su}{(u-m_{\tilde g}^2)^2}+\frac{sm_{\tilde g}^2}{(t-m_{\tilde g}^2)^2}+\frac{sm_{\tilde g}^2}{(u-m_{\tilde g}^2)^2}\delta_{ij}-\frac{2sm_{\tilde g}^2}{3(t-m_{\tilde g}^2)(u-m_{\tilde g}^2)}\delta_{ij}\right], \tag{199}$$

where m_i and m_j are the masses of the produced squarks, and $m_{\tilde g}$ is the gluino mass.

For the reaction $q_i\bar q_j\to\tilde q_i\tilde q_j^*$ the differential cross section is

$$\frac{d\sigma}{dt}(q_i\bar q_j\to\tilde q_i\tilde q_j^*)=\frac{4\pi\alpha_s^2}{9s^2}\left[\left[\frac{ut-m_i^2m_j^2}{s^2}\right]\left[\delta_{ij}\left[2-\frac{2}{3}\frac{s}{(t-m_{\tilde g}^2)}\right]+\frac{s^2}{(t-m_{\tilde g}^2)^2}\right]+\frac{sm_{\tilde g}^2}{(t-m_{\tilde g}^2)^2}\right]. \tag{200}$$

For the reaction $gg\to\tilde q_i\tilde q_i^*$ the differential cross section is

$$\frac{d\sigma}{dt}(gg\to\tilde q_i\tilde q_i^*)=\frac{\pi\alpha_s^2}{s^2}\left[\frac{7}{48}+\frac{3(u-t)^2}{16s^2}\right]\left[1+\frac{2m^2t}{(t-m^2)^2}+\frac{2m^2u}{(u-m^2)^2}+\frac{4m^4}{(t-m^2)(u-m^2)}\right]. \tag{201}$$

Here m is the mass of the corresponding squark (we assume that the left- and right-handed squarks are degenerate in mass).

The differential cross section for the reaction $gq_i\to\text{gaugino}+\tilde q_i$ is

$$\frac{d\sigma}{dt}(gq_i\to\text{gaugino}+\tilde q_i)=\frac{\pi}{s^2}\left[B_s\frac{(\mu^2-t)}{s}+B_t\frac{[(\mu^2-t)s+2\mu^2(m_i^2-t)]}{(t-\mu^2)^2}+B_u\frac{(u-\mu^2)(u+m_i^2)}{(u-m_i^2)^2}+B_{st}\frac{[(s-m_i^2+\mu^2)(t-m_i^2)-\mu^2s]}{s(t-\mu^2)}+B_{su}\frac{[s(u+\mu^2)+2(m_i^2-\mu^2)(\mu^2-u)]}{s(u-m_i^2)}+B_{tu}\frac{[(m_i^2-t)(t+2u+\mu^2)+(t-\mu^2)(s+2t-2m_i^2)+(u-\mu^2)(t+\mu^2+2m_i^2)]}{2(t-\mu^2)(u-m_i^2)}\right], \tag{202}$$

where μ is the mass of the gauge fermion, and m_i is the mass of the scalar quark. The coefficients B_x are given in the paper of Eichten *et al.*[4] For instance, for the case in which gaugino≡gluino the coefficients B_x are: $B_s=(4\alpha_s^2/9)\delta_{ij}$, $B_t=\frac{9}{4}B_s$, $B_u=B_s$, $B_{st}=-B_t$, $B_{su}=\frac{1}{8}B_s$, $B_{tu}=\frac{9}{8}B_s$.

We consider finally the production of sleptons. The differential cross section for production of charged slepton–sneutrino pairs is

$$\frac{d\sigma}{dt}(d\bar u\to W\to\tilde l_L\bar{\tilde\nu}_L)=\frac{g_2^4|D_W(s)|^2}{192\pi s^2}(tu-m_{\tilde l_L}^2m_{\tilde\nu_L}^2). \tag{203}$$

For $\tilde l_L$ pair production the differential cross section is

$$\frac{d\sigma}{dt}(q\bar q\to\gamma^*,Z\to\tilde l_L\bar{\tilde l}_L)=\frac{2\pi\alpha^2}{3s^2}[tu-m_{\tilde l_L}^4]\times\left[\frac{q_l^2q_q^2}{s^2}+(\alpha_l-\beta_l)^2(\alpha_q^2+\beta_q^2)|D_Z(s)|^2+\frac{2q_lq_q\alpha_q(\alpha_l-\beta_l)(s-M_Z^2)}{s}|D_Z(s)|^2\right], \tag{204}$$

where $D_V(s)=1/(s-M_V^2+iM_V\Gamma_V)$, $q_l=-1$, $q_\nu=0$, $q_u=2/3$, $q_d=-1/3$, $\alpha_l=\frac{1}{4}(3t-c)$, $\alpha_\nu=\frac{1}{4}(c+t)$, $\alpha_u=-\frac{5}{12}t+\frac{1}{4}c$, $\alpha_d=-\frac{1}{4}c+\frac{1}{12}t$, $\beta_l=\frac{1}{4}(c+t)$, $\beta_\nu=-\frac{1}{4}(c+t)$, $\beta_u=-\frac{1}{4}(c+t)$, $\beta_d=\frac{1}{4}(c+t)$, $c=\cot\theta_W$, $t=\tan\theta_W$. The differential cross section for sneutrino pair production can be obtained by the replacement of α_l, β_l, q_l, and $m_{\tilde l}$ by α_ν, β_ν, 0, and $m_{\tilde\nu}$, respectively, whereas for $\tilde l_R$ pair production one must substitute $\alpha_l-\beta_l\to\alpha_l+\beta_l$ and $m_{\tilde l_L}\to m_{\tilde l_R}$.

Superparticle decays. The decay widths of the superparticles depend rather strongly on the relations between the superparticle masses. Here we outline the main decay channels only. The formulas for the decay widths are given in Ref. 49. We consider first the decays of gluinos and squarks. For $m_{\tilde{g}} > m_{\tilde{q}}$ the main decays are

$$\tilde{g} \to \tilde{q}_i \bar{q}_i, \ \bar{\tilde{q}}_i q_i, \tag{205}$$

$$\tilde{q}_k \to \chi_i^0 q_k, \tag{206}$$

$$\tilde{q}_k \to \chi_j^+ q_m, \chi_j^- q_l. \tag{207}$$

For $m_{\tilde{g}} < m_{\tilde{q}}$ the main decays are

$$\tilde{q}_i \to \tilde{g} q_i, \tag{208}$$

$$\tilde{g} \to q \bar{q}' \chi_k^+, \tag{209}$$

$$\tilde{g} \to q' \bar{q} \chi_k^-, \tag{210}$$

$$\tilde{g} \to q \bar{q} \chi_k^0. \tag{211}$$

The charginos and neutralinos are usually assumed to be lighter than gluinos and squarks, and their main decays are

$$\chi_i^0 \to \chi_j^0 + Z, \tag{212}$$

$$\chi_i^0 \to \chi_j^\pm + W^\mp, \tag{213}$$

$$\chi_i^\pm \to \chi_j^0 + W^\pm, \tag{214}$$

$$\chi_i^\pm \to \chi_j^\pm + Z. \tag{215}$$

The two-body decays of neutralinos and charginos into Higgs bosons are

$$\chi_i^0 \to \chi_j^0 + h(H), \tag{216}$$

$$\chi_i^0 \to \chi_k^\pm + H^\mp, \tag{217}$$

$$\chi_i^\pm \to \chi_k^0 + H^\pm, \tag{218}$$

$$\chi_i^\pm \to \chi_j^\pm + h(H). \tag{219}$$

The left sleptons decay dominantly via gauge interactions into charginos or neutralinos via two-body decays:

$$\tilde{l}_L \to l + \chi_i^0, \tag{220}$$

$$\tilde{l}_L \to \nu_L + \chi_j^-, \tag{221}$$

$$\tilde{\nu}_L \to \nu_L + \chi_i^0, \tag{222}$$

$$\tilde{\nu}_L \to l + \chi_j^+. \tag{223}$$

For relatively light sleptons, only decays into the LSP are possible, so that light sneutrino decays are invisible. Heavier sleptons can decay via the chargino or other (non-LSP) channels. These decays are important because they proceed via the larger $SU(2)$ gauge coupling constant and can dominate the direct decay to the LSP. The $SU(2)$ singlet charged sleptons $\tilde{l}_R$ decay only via their $U(1)$ gauge interactions, and in the limit of vanishing Yukawa coupling their decays to charginos are forbidden. Therefore, the main decay mode of the right-handed slepton is

$$\tilde{l}_R \to l + \chi_i^0. \tag{224}$$

In many cases the mode into the LSP dominates.

Let us now briefly describe the main signatures for the search for sparticles at LHC. Sparticle pair production at LHC is followed by sparticle decays until the LSP is reached. Therefore, the main signature of sparticle production is events with $(n \geq 0)$ jets plus $m \geq 0$ isolated leptons plus missing transverse energy due to escape from detector registration of two LSPs. It is natural to divide the signatures into the following categories:[50]

(a) multijets plus E_t^{miss} events;
(b) $1l$ plus jets plus E_t^{miss} events;
(c) $2l$ plus jets plus E_t^{miss} events;
(d) $3l$ plus jets plus E_t^{miss} events;
(e) $4l$ plus jets plus E_t^{miss} events;
(f) $\geq 5l$ plus jets plus E_t^{miss} events.

Multileptons arise as a result of cascade decays of neutralinos and charginos into W and Z bosons with subsequent decays of W and Z bosons into leptonic modes. For instance, same-sign dilepton events arise as a result of the cascade decay

$$\tilde{g} \to q' \bar{q} \chi^\pm, \quad \chi^\pm \to W^\pm \chi_1^0 \to l^\pm \nu \chi_1^0, \tag{225}$$

where l stands for either e or μ. Opposite-sign dilepton events can arise as a result of the cascade decay

$$\tilde{g} \to q \bar{q} \chi_i^0, \quad \chi_i^0 \to Z \chi_1^0 \to l^+ l^- \chi_1^0. \tag{226}$$

It should be noted that multilepton supersymmetry signatures arise as a result of decays of squarks or gluinos into charginos or neutralinos which are different from the LSP with subsequent decays of charginos or neutralinos into (W,Z) bosons plus the LSP. Leptonic decays of (W,Z) bosons is the origin of leptons. However, for the case of nonuniversal gaugino mass relations at the GUT scale it is possible to realize the situation[42] when all charginos and neutralinos are heavier than the gluinos and squarks. Therefore, gluinos and squarks will decay mainly into quarks or gluons plus the LSP, so that cascade decays and, as a consequence, multilepton events will be absent.

3.3.2. The search for SUSY Higgs bosons

In the MSSM there are four Higgs bosons $(h,H,A,H^\pm)$. As has been mentioned before, at the tree level the lightest Higgs-boson mass is predicted to be less than m_Z. However, inclusion of radiative corrections for a large top-quark mass (which occurs in reality) can increase the Higgs-boson mass up to 120 GeV for a stop mass equal to 1 TeV. From the vacuum-stability bound[15] the standard Higgs-boson mass for $m_t \geq 175$ GeV is predicted to be greater than 120 GeV. This means that the predictions for the Higgs-boson mass in the MSSM and SM lie in different mass intervals; i.e., knowledge of the Higgs-boson mass would enable us to discriminate between the MSSM and the SM. In particular, the discovery of a light Higgs boson at LEP2 would be powerful nontrivial evidence in favor of low-energy broken supersymmetry.

$h,H \to \gamma\gamma$. In the MSSM, the neutral Higgs boson remains extremely narrow in the kinematic region where the two-photon decay has a reasonable branching ratio. The experimental requirements and backgrounds are the same as in

the case of the standard Higgs boson decaying into two photons. Therefore, the ECAL mass resolution and acceptance are crucial for the discovery of the Higgs boson. In the case where the SUSY masses are larger than $O(300)$ GeV the $h\to\gamma\gamma$ branching ratio in the MSSM coincides with the corresponding branching ratio of the SM, so that we have in fact the same significance as in the case of the SM. We shall consider the limiting case where the sparticle masses are sufficiently heavy and do not play an important role in Higgs-boson decays. The decay channels for the MSSM lightest Higgs boson will then be the same as for the SM Higgs boson, but the production rates will be significantly modified by the MSSM couplings. There are two main production processes for the MSSM neutral Higgs bosons: $gg\to h(H)$ and $gg\to h(H)b\bar{b}$. The second mechanism is important at large $\tan\beta$, due to the enhanced $h(H)b\bar{b}$ couplings. These associated-production processes are interesting, as b-tagging techniques may be able to enhance the signal-to-background ratio, possibly allowing the observation of h, H, and A.[51]

$H\to ZZ^*$, ZZ and $h\to ZZ^*$. The scalar Higgs bosons H and h couple to W and Z boson pairs, and so can be sought in 4-lepton final states from the processes h, $H\to ZZ^*$, ZZ. The regions of the MSSM $(\tan\beta, m_A)$ space [$\tan\beta = \langle H_t\rangle/\langle H_b\rangle$; m_A is the mass of the axial Higgs boson] in which Higgs bosons could be discovered through four-lepton modes are divided into the region of low $\tan\beta$, where H could be discovered, and the region of high $\tan\beta$, where only h could be discovered.

h, H, $A\to\tau\bar{\tau}\to l^{\pm}h^{\pm}+X$. The $\tau\bar{\tau}$ final states can be sought in a "lepton+hadron" final state or in an $e+\mu$ final state. For the one-lepton plus one-hadron final states, intermediate backgrounds are due to Z, $\gamma^*\to\tau\bar{\tau}$; $t\bar{t}\to\tau\bar{\tau}+X$, $\tau+X$; $b\bar{b}\to\tau\bar{\tau}+X$, τX. Reducible backgrounds are due to events with one hard lepton and jets with a jet misidentified as a τ. Typical cuts are the following:[1]

1. One isolated lepton with $p_T\geqslant(15-40)$ GeV, depending on the axial Higgs-boson mass m_A and $|\eta|\leqslant 2$.

2. One τ-jet candidate which contains only one charged hadron.

3. No other significant jet activity.

An overall lepton reconstruction of 90% is assumed. For the $\tau\bar{\tau}\to e^{\pm}+\mu^{\mp}$ final states a pair of opposite-sign isolated electrons and muons with $p_T\geqslant 20$ GeV and $|\eta|\leqslant 2$ is required. There can be large backgrounds from Z, $\gamma^*\to\tau\bar{\tau}$, $t\bar{t}$, $b\bar{b}$, W^+W^-. The $t\bar{t}$ and W^+W^- backgrounds can be reduced to the level of $\approx 20\%$ of the Z, γ^* backgrounds. Roughly speaking, A, H bosons can be discovered using these modes with masses up to 600 GeV.

Charged Higgs $H^{\pm}$ in the processes $t\to H^{\pm}h$, $H^{\pm}\to\tau\nu_{\tau}$. In the MSSM the top quark can decay to a charged Higgs ($t\to H^+b$). The $t\to H^+b$ branching ratio is large at low and high $\tan\beta$ values, with a minimum at $\tan\beta\approx 6$. The H^+ has two main decay modes, $H^+\to c\bar{s}$ and $H^+\to\tau^+\nu_{\tau}$. The $H^+\to\tau^+\nu_{\tau}$ branching is large for $\tan\beta\geqslant 2$, and depends only slightly on $\tan\beta$.

h, H, $A\to\mu^+\mu^-$. In the SM and in the MSSM for interesting values of the Higgs-boson masses the $H\to\mu^+\mu^-$ branching ratio is small, $\approx 3\times 10^{-4}$. For the SM Higgs boson the main background is the Drell–Yan production process γ^*, $Z\to\mu^+\mu^-$. However, in the MSSM the $\mu^+\mu^-$ channel could be very interesting for large values of $\tan\beta$. It appears that for $m_A\leqslant 200$ GeV and $\tan\beta\geqslant 2.5$ for integrated luminosity 10^4 pb^{-1} it is possible to discover A and H bosons at the level $\geqslant 7\sigma$. The discovery potential of the Higgs boson for this mode at $L=10^5$ pb^{-1} is similar to the discovery potential of the Higgs boson for the standard mode H, h, $A\to\tau\tau$ for 10^4 pb^{-1}. However, the $\mu^+\mu^-$ channel gives much better signal identification and mass resolution.[1]

h, H, A in associated production of $b\bar{b}H_{\text{susy}}$. While $gg\to b\bar{b}H$ associated production is negligible for the SM Higgs boson in comparison with ttH in the MSSM, the rate of $gg\to b\bar{b}H_{\text{susy}}$ is 30–50% of the total production for $m_A=100$ GeV and 70–80% for $m_A=300$ GeV with $\tan\beta=10-30$. The signal-to-background ratio can be enhanced by b tagging.

$A\to Zh\to b\bar{b}b\bar{b}$. The large branching ratio ($\approx 50\%$) of $A\to Zh$ in the region $\tan\beta\leqslant 2$ for 180 GeV$\leqslant m_A\leqslant 2m_t$ could allow the observation of A and h in this region.

The main conclusion concerning the search for MSSM Higgs bosons for different $(m_A, \tan\beta)$ values is that Higgs bosons for $m_A\leqslant 500$ GeV would be detectable at CMC, except that this may be very difficult in the region 110 GeV $\leqslant m_A\leqslant 200$ GeV, $3\leqslant\tan\beta\leqslant 10$ and in the smaller region $\tan\beta\approx 2.5$ and 200 GeV$\leqslant m_A\leqslant 280$ GeV. The most promising channel for these regions is h, $H\to b\bar{b}$, from Wh, Zh, and $t\bar{t}h$ final states.

3.3.3. Squark and gluino search

Jets+E_T^{miss} channel. There are many possible scenarios, depending on the concrete values of the squark and gluino masses, for the search for squarks and gluinos using this signature. We consider two typical scenarios.[1]

Scenario A. $m_{\tilde{b}}$, $m_{\tilde{t}}\leqslant m_{\tilde{g}}$.

In this case the two-body decay $\tilde{g}\to\tilde{b}\bar{b}$ with $\tilde{b}\to\chi_1^0 b$ dominates, because the top is too massive to allow $\tilde{g}\to\tilde{t}\bar{t}$ decay. Thus, the resulting event signature will have four b jets in the final state.

Scenario B. $m_{\tilde{q}}=m_{\tilde{g}}$.

In this scenario the gluino decays directly into the LSP ($\tilde{g}\to q\bar{q}\chi_1^0$), leading to the typical E_T^{miss}+multijets final-state event topology without an excess of b jets.

In the scenario with heavy squarks and gluinos ($m_{\tilde{q}}=1550$ GeV, $m_{\tilde{g}}=1500$ GeV), after using some cuts we have $N_{\text{ev}}/N_{\text{back}}\sim 8.5$. In general, for an integrated luminosity of 10^5-10^3 pb^{-1}, the sensitivity to the channel of multijets+missing energy can be expressed as the following accessibility for the gluino mass $m_{\tilde{g}}$:[2]

$m_{\tilde{g}}\leqslant 1600(1050)$ GeV for $m_{\tilde{q}}=2m_{\tilde{g}}$;

$m_{\tilde{g}}\leqslant 2300(1800)$ GeV for $m_{\tilde{q}}=m_{\tilde{g}}$;

$m_{\tilde{g}}\leqslant 3600(2600)$ GeV for $m_{\tilde{q}}=m_{\tilde{g}}/2$.

Lepton(s)+E_t^{miss}+jets. Cascade decays of squarks and gluinos are an important source of leptons. Therefore, events with E_t^{miss}+jets+lepton(s) provide a good signature for searching for gluinos and squarks over a wide mass range.

Four event classes, which contain one to three leptons (muons or electrons), give important signatures for the search for squarks and gluinos:

$1l$: a single lepton$+E_t^{\text{miss}}+$jets;

$2l$: two leptons with opposite charges$+E_t^{\text{miss}}+$jets;

$2l(ss)$: same-sign dileptons$+E_t^{\text{miss}}+$jets;

$3l$: three dileptons$+E_t^{\text{miss}}+$jets.

The background comes from $t\bar{t}$, $W+$jets, $Z+$jets, WW, and WZ. The main conclusion[52] is that the signature with a single lepton$+E_t^{\text{miss}}$ gives the most powerful restriction on the gluino mass for the search for SUSY at the CMS detector. Namely, for L_t from 10^4 pb^{-1} to 10^5 pb^{-1} the CMS will be capable of discovering gluinos from 1.5 TeV up to 2 TeV and squarks from 1.5 TeV up to 2.3 TeV. Another conclusion is that the mass limits for discovery of the gluino and squark are not very sensitive to the increase in the SM background.

3.3.4. Neutralino and chargino search

Chargino and neutralino pairs, produced through the Drell–Yan mechanism or squark exchange, may be detected through their leptonic decays $\chi_1^{\pm}$, $\chi_2^0 \to lll + E_T^{\text{miss}}$. The leptonic decays of $\chi_1^{\pm}$ and χ_2^0 are

$$\chi_1^{\pm} \to \chi_1^0 l^{\pm} \nu,$$

$$\chi_1^{\pm} \to (\tilde{l}_{L,R}^{\pm} \to \chi_1^0 l^{\pm}) \nu,$$

$$\chi_1^{\pm} \to (\tilde{\nu}_L \to \chi_1^0 \nu) l^{\pm},$$

$$\chi_1^{\pm} \to (W^{\pm} \to l^{\pm} \nu) \chi_1^0,$$

$$\chi_2^0 \to \chi_1^0 l^+ l^-,$$

$$\chi_2^0 \to (\tilde{l}_{L,R}^{\pm} \to \chi_1^0 l^{\pm}) l^{\mp},$$

$$\chi_2^0 \to (\chi_1^{\pm} \to \chi_1^0 l^{\pm} \nu) l^{\mp} \nu.$$

The three-lepton signal is produced through the decay chain $\chi_1^{\pm} \to l^{\pm} + \chi_1^0$ and $\chi_2^0 \to ll + \chi_1^0$, where the undetected neutrino and χ_1^0 produce E_T^{miss}. The main backgrounds to this channel arise from WZ/ZZ, $t\bar{t}$, $Zb\bar{b}$, and $b\bar{b}$ production. In principle, there could be a SUSY background arising from squark and gluino cascade decays into multileptonic modes.

Typical cuts are the following:[53]

(i) Three isolated leptons with $p_t^l > 15$ GeV.

(ii) Veto central jets with $E_t > 25$ GeV in the interval $|\eta| < 3.5$.

(iii) $m_{l\bar{l}} < 81$ GeV or $m_{l\bar{l}} \neq M_Z \pm \delta M_Z$.

The main conclusion is that neutralinos and charginos could be detected, provided that their masses are lighter than 350 GeV.[53] Moreover, it is possible to determine the $M(\chi_2^0) - M(\chi_1^0)$ mass difference by measurement of the distribution in the l^+l^- invariant mass arising from the decay $\chi_2^0 \to \chi_1^0 + l^+ l^-$ (Ref. 53).

3.3.5. Slepton search

Slepton pairs produced by the Drell–Yan mechanism can be detected through their leptonic decays $\tilde{l} \to l + \chi_1^0$. In the final state we then expect a dilepton pair with missing energy and no hadronic jets. Here we shall use the results of Ref. 54, where concrete estimates were made for the CMS detector. We consider two points of Ref. 54:

Point A: $m(\tilde{l}_L) = 314$ GeV, $m(\tilde{l}_R) = 192$ GeV, $m(\tilde{\nu}) = 308$ GeV, $m(\chi_1^0) = 181$ GeV, $m(\chi_2^0) = 358$ GeV, $m(\tilde{g}) = 1036$ GeV, $m(\tilde{q}) = 905$ GeV, $\tan\beta = 2$, $\text{sign}(\mu) = -1$.

Point B: $m(\tilde{l}_L) = 112$ GeV, $m(\tilde{l}_R) = 98$ GeV, $m(\tilde{\nu}) = 93$ GeV, $m(\chi_1^0) = 39$ GeV, $m(\chi_2^0) = 87$ GeV, $m(\tilde{g}) = 254$ GeV, $m(\tilde{q}) = 234$ GeV, $\tan\beta = 2$, $\text{sign}\,\mu = -1$.

For point A the following cuts were used: $p_t^l \geq 50$ GeV, Isol ≤ 0.1, $|\eta| \leq 2.5$, $E_t^{\text{miss}} \geq 120$ GeV, $\Delta\phi(E_t^{\text{miss}}, ll) \geq 150°$, jet veto—no jets with $E_t^{\text{jet}} \geq 30$ GeV for $|\eta| \leq 4.5$, Z-mass cut ($M_Z \pm 5$ GeV excluded), $\Delta\phi(l^+l^-) \leq 130°$.

With such cuts for the total luminosity $L_t = 10^5$ pb^{-1}, 91 events with $e^+e^- + \mu^+\mu^-$ resulting from slepton decays were found. The standard WS-model background comes from WW, $t\bar{t}$, $Wt\bar{b}$, $WZ\tau\bar{\tau}$ and gives 105 events. No SUSY background was found. The significance $S = \text{sleptons}/\sqrt{\text{background} + \text{sleptons}}$ for slepton discovery at the point A is $S = 6.5$.

For point B the cuts are similar to those of point A, except that we have $p_t^l \geq 20$ GeV, $E_t^{\text{miss}} \geq 50$ GeV, $\Delta\phi(E_t^{\text{miss}}, ll) \geq 160°$. For the total luminosity $L_t = 10^4$ pb^{-1} the number of $e^+e^- + \mu^+\mu^-$ events resulting from direct slepton production was found to be 323. The number of background events was estimated as 989 (standard model background) + 108 (SUSY background) = 1092. The significance is $S = 8.6$.

The main conclusion of Ref. 54 is that for $L_t = 10^5$ pb^{-1} the CMS will be capable of discovering sleptons with masses up to 400 GeV.

The search for flavor lepton-number violation in slepton decays. In supersymmetric models with explicit flavor lepton-number violation due to soft supersymmetry-breaking terms there could be detectable flavor lepton-number violation in slepton decays.[55] For instance, for the case of nonzero mixing $\sin\phi \neq 0$ between right-handed selectrons and smuons we have flavor lepton-number violation in slepton decays, namely,[55]

$$\Gamma(\tilde{\mu}_R \to \mu + \text{LSP}) = \Gamma \cos^2\phi, \tag{227}$$

$$\Gamma(\tilde{\mu}_R \to e + \text{LSP}) = \Gamma \sin^2\phi, \tag{228}$$

$$\Gamma(\tilde{e}_R \to e + \text{LSP}) = \Gamma \cos^2\phi, \tag{229}$$

$$\Gamma(\tilde{e}_R \to \mu + \text{LSP}) = \Gamma \sin^2\phi, \tag{230}$$

$$\Gamma = \frac{g_1^2}{8\pi}\left(1 - \frac{M_{\text{LSP}}^2}{M_{\text{SL}}^2}\right)^2. \tag{231}$$

A typical prediction of the nonzero smuon–selectron mixing is the existence of noncoplanar $e^{\pm}\mu^{\mp}$ signal events with missing energy arising from production of slepton pairs, which subsequently decay with flavor lepton-number violation. The possibility of detecting flavor lepton-number violation in slepton decays at LHC was discussed in Ref. 56. The main conclusion is that for the most optimistic case of the maximal mixing $\sin\phi = 1/\sqrt{2}$ it would be possible to discover

slepton mixing at LHC for the points A and B, which have been considered for the case of zero slepton mixing in Ref. 54.

3.4. The search for physics beyond the SM and MSSM

Search for new vector bosons. Many string-inspired supersymmetric electroweak models and grand unified models based on extended gauge groups $[SO(10),E_6,\ldots]$ predict the existence of new, relatively light, neutral Z' bosons. The main mechanism for the production of such new neutral vector bosons is quark–antiquark fusion. The cross section is given by the standard formula

$$\sigma(pp\to Z'+\ldots)=\sum_i \frac{12\pi^2\Gamma(Z'\to\bar{q}_iq_i)}{9M_{Z'}s}\int_{M^2_{Z'}/s}^1\frac{dx}{x}\times[\bar{q}_{pi}(x,\mu)q_{pi}(x^{-1}M^2_{Z'}s^{-1},\mu)+q_{pi}(x,\mu)\bar{q}_{pi}(x^{-1}M^2_{Z'}s^{-1},\mu)]. \quad (232)$$

Here $\bar{q}_{pi}(x,\mu)$ and $q_{pi}(x,\mu)$ are the parton distributions of the antiquark $\bar{q}_i$ and quark q_i in the proton at the normalization point $\mu\sim M_{Z'}$, and $\Gamma(Z'\to\bar{q}_iq_i)$ is the hadronic width for decay of the Z' boson into a quark–antiquark pair with flavor i. In most models, as a result of the γ_5 anomaly cancellation, the Z' boson interacts with quarks and leptons, and therefore the best signature for the search for the Z' boson is through its decay to electron pairs, muon pairs, and jet pairs. The LHC Z'-boson discovery potential depends on the couplings of the Z' boson to the quarks and leptons. For a Z' boson decaying into a lepton pair the main background comes from the Drell–Yan process, which is under control. For a Z' with quark and lepton couplings equal to the Z couplings to the quarks and leptons it would be possible to discover a Z' boson with mass up to 5 TeV.[2]

Many extended gauge electroweak models based, for instance, on the gauge group $SU(2)_L\otimes SU(2)_R\otimes U(1)$ predict the existence of an additional charged vector W' boson. The main production mechanism for the W' boson is quark–antiquark fusion similar to that in the case of Z' production. The best way to look for the W' boson is through its leptonic mode $W'\to l\nu$.

For the model with a right-handed charged W' boson it would be possible to discover the W' boson through the leptonic mode $W'\to e\nu$ with a W' mass up to 6 TeV.[2] The typical accuracy in the determination of the W' mass is 50–100 GeV.

Search for supersymmetry with R-parity violation. Most supersymmetric phenomenology assumes the MSSM, which conserves R parity. As a result of R-parity conservation, supersymmetric particles can be produced only in pairs, and a supersymmetric state cannot decay into conventional states. This has a nontrivial consequence for the search for supersymmetric particles at supercolliders; in particular, all experimental searches for SUSY rely on pair production and on missing transverse momentum $p_t^{\rm miss}$ as a signal for the production of the LSP, which must be stable and electrically neutral. However, at present, there are no deep theoretical motivations in favor of R-parity conservation. The phenomenology of the models, with explicit R violation at hadron colliders, has been studied in Ref. 57. The most general trilinear terms in the superpotential explicitly violating R parity have the form[57]

$$W_{R,br}=\lambda_{ijk}L_iL_j\bar{E}_k+\lambda'_{ijk}L_iQ_j\bar{D}_k+\lambda''_{ijk}\bar{U}_i\bar{D}_j\bar{D}_k, \quad (233)$$

where L and $\bar{E}$ (Q and $\bar{U}$, $\bar{D}$) are the (left-handed) lepton doublet and the antilepton singlet (quark doublet and antiquark singlets) chiral superfields, respectively. The terms of (233) violate baryon and lepton number and, if present in the Lagrangian, generate an unacceptably large amplitude for proton decay, which is suppressed only by the square of the inverse squark mass. The R parity prohibits the dangerous terms (233) in the superpotential. However, R parity is not the only way to construct a minimal supersymmetric extension of the standard model. It is easy to give alternatives to R-parity symmetries, which allow for a different set of couplings. For example, under the transformation

$$(Q,\bar{U},\bar{D})\to-(Q,\bar{U},\bar{D}),\ (L,\bar{E},H_{1,2})\to+(L,\bar{E},H_{1,2}) \quad (234)$$

only the quark superfields change sign. If the Lagrangian is invariant under the transformations (234), then only the last, baryon-number violating term in (233), $\bar{U}\bar{D}\bar{D}$, is forbidden. This gives a new model, in which a single supersymmetric state can couple to standard-model states breaking R parity. Similarly, there are analogous transformations forbidding the lepton-number violating terms.

In the direct search for supersymmetric particles the phenomenology is altered considerably when R-parity violating terms are included in the superpotential. In general, both the production mechanisms and the decay patterns can change. In addition to the standard supersymmetric pair production of particles, there is now the possibility of production of R-odd final states as well. Moreover, if all supersymmetric particles decay in the detector, we will no longer have the standard $p_t^{\rm miss}$ signal, and the decay patterns will all be altered. In particular, the LSP will decay mainly into three-body final states.[57] However, except for the LSP, which now decays, all particles decay predominantly as in the MSSM. Consider the case in which the LSP decays within the detector. For the model with R-parity breaking terms involving leptonic superfields we expect additional lepton pairs in the final state as a result of the LSP decay. Therefore, we expect, instead of the missing-energy signature, the presence of additional lepton pairs in comparison with the standard MSSM signatures, which in principle is more visible at LHC than the SUSY signatures in the MSSM. The $\bar{U}\bar{D}\bar{D}$ operators, however, lead to less characteristic signals, but for cascade decays they lead to signals comparable to those in the MSSM.

Note that it is possible to construct a model with supersmall R-parity violation and with a relatively long-lived ($t\sim10^{-1}-10^{-9}$ sec) charged $\tilde{\tau}_R$ slepton that plays the role of the LSP.[59] The relatively long-lived charged LSP penetrates through the detector, and it is possible to detect it by a track measurement.

Search for leptoquarks. At LHC the leptoquark pair production proceeds predominantly through gg fusion, which does not involve any lepton–quark–leptoquark vertex

and is therefore predicted with $\approx 50\%$ accuracy. In 25% of the events, the final state contains two electrons and two jets. The dominant background in this case is from $t\bar{t}$ production. The conclusion is that leptoquarks with masses up to 1 TeV will be discovered at LHC.

Search for scalar color octets. Relatively light [$M_8 \leq O(1)$ TeV] scalar $SU_c(3)$ color $SU_L(2)\otimes U(1)$ neutral octets are predicted in some supersymmetric and nonsupersymmetric GUTs.[61] Light scalar octets arise naturally in models with large compactification radius of the additional space dimensions.

To be precise, consider light scalar octets that are neutral under the $SU_L(2)\otimes U(1)$ electroweak gauge group. Such particles are described by the self-conjugate scalar field $\Phi^\alpha_\beta(x)$ [$(\Phi^\alpha_\beta(x))^* = \Phi^\beta_\alpha(x)$, $\Sigma_\alpha \Phi^\alpha_\alpha(x) = 0$], and they interact only with gluons. Here $\alpha = 1,2,3$ and $\beta = 1,2,3$ are $SU(3)$ indices. The scalar potential for the scalar octet field $\Phi^\alpha_\beta(x)$ has the form

$$V(\Phi) = \frac{M^2}{2}\,\mathrm{Tr}(\Phi^2) + \frac{\lambda_1 M}{6}\,\mathrm{Tr}(\Phi^3) + \frac{\lambda_2}{12}\,\mathrm{Tr}(\Phi^4) + \frac{\lambda_3}{12}\,\mathrm{Tr}(\Phi^2)^2. \tag{235}$$

The term $(\lambda_1 M/6)\,\mathrm{Tr}(\Phi^3)$ in the scalar potential (235) breaks the discrete symmetry $\Phi \to -\Phi$. The existence of such a term in the Lagrangian leads to decay of the scalar octet mainly into two gluons through one-loop diagrams similar to the corresponding one-loop diagrams describing the Higgs-boson decay into two photons. One finds that the width for decay of the scalar octet into two gluons is determined by the formula[60]

$$\Gamma(\Phi \to gg) = \frac{15}{4096\pi^3}\,\alpha_s^2 c^2 \lambda_1^2 M, \tag{236}$$

where

$$c = \int_0^1 \int_0^{1-w} du\,dw\,\frac{wu}{1-u-w} \simeq 0.48 \tag{237}$$

and α_s is the effective coupling constant at some normalization point $\mu \sim M$. Numerically, for $\alpha_s = 0.12$ we find

$$\Gamma(\Phi \to gg) = 0.4 \times 10^{-8} \lambda_1^2 M. \tag{238}$$

From the requirements that the color $SU(3)$ symmetry is unbroken (the minimum $\langle \Phi^\alpha_\beta(x) \rangle = 0$ is the deepest one), and that the effective coupling constants $\bar{\lambda}_2$ and $\bar{\lambda}_3$ do not have a Landau pole singularity up to the energy $M_0 = 100M$ we find that $\lambda_1 \leq O(1)$. Therefore, the decay width of the scalar color octet is less than $O(1)$ keV or $O(10)$ keV for the octet masses 100 and 1000 GeV, respectively. This means that new hadrons composed of the scalar octet Φ, quarks, and gluons ($g\Phi, \bar{q}\Phi q, qqq\Phi$) are relatively long-lived even for high scalar-octet mass. Consider the pair production of scalar octets at LHC. The corresponding lowest-order parton cross sections have the form[60]

$$\frac{d\sigma}{dt}(\bar{q}q \to \Phi\Phi) = \frac{4\pi\alpha_s^2}{3s^4}(tu - M^4), \tag{239}$$

$$\frac{d\sigma}{dt} = \frac{\pi\alpha_s^2}{s^2}\left(\frac{81}{96} + \frac{9(u-t)^2}{32s^2}\right)\left(1 + \frac{2M^2}{u-M^2} + \frac{2M^2}{t-M^2} + \frac{2M^4}{(u-M^2)^2} + \frac{2M^4}{(t-M^2)^2} + \frac{4M^4}{(t-M^2)(u-M^2)}\right), \tag{240}$$

$$\sigma(\bar{q}q \to \Phi\Phi) = \frac{2\pi\alpha_s^2}{9s}\,k^3, \tag{241}$$

$$\sigma(gg \to \Phi\Phi) = \frac{\pi\alpha_s^2}{s}\left(\frac{15k}{16} + \frac{51kM^2}{8s} + \frac{9M^2}{2s^2}(s - M^2)\ln\left(\frac{1-k}{1+k}\right)\right), \tag{242}$$

where $k = (1 - 4M^2/s)^{1/2}$. At LHC the main contribution ($\geq 95\%$) for the production of scalar octets comes from gluon annihilation into two scalar octets, $gg \to \Phi\Phi$. The scalar octets decay into two gluons, which leads to four-jet events at LHC. Therefore, the only signature of scalar octets at LHC is four-jet events. The main background comes from QCD four-jet events. The cross section for scalar-octet production is typically $O(10^{-4})$ of the standard QCD two-jet cross section, and $O(10^{-2})$ of the four-jet QCD background. The preliminary conclusion is that at LHC for $L_t = 10^5$ pb^{-1} it would be possible to discover scalar octets with mass $M \leq 900$ GeV.

Search for Kaluza–Klein states. As is well known, new degrees of freedom are required in any attempt at unification of the electroweak and strong interactions with gravity. Among such attempts, only superstring theory is known to provide a consistent description of quantum gravity. Strings predict two kinds of new degrees of freedom:

(i) Superheavy oscillation modes, whose characteristic scale is given by the inverse string tension, $(\alpha')^{-1/2} \sim 10^{18}$ GeV. These states are important at very short distances of the order of the Planck length, and they modify the ultraviolet behavior of gravitational interactions.

(ii) States associated with the internal compactified space, whose presence is required by the fact that superstring theory in flat space is anomaly-free only in ten dimensions. Usually, the size of the internal space is also made too small to give any observable effect in particle accelerators.

However, it is possible to construct superstring models having one or two large internal dimensions at a scale accessible to LHC.[61] The presence of such large dimensions is motivated by superstring theory with perturbative breaking of supersymmetry,[62] and their size is inversely proportional to the scale of supersymmetry breaking, which must be of the order of the electroweak scale in order to protect the gauge hierarchy. In contrast to field-theoretical expectations, string theory allows the existence of such large dimension(s) consistently with perturbative unification of low-energy couplings in a class of models based on orbifold compactifications.[63] Properties of string models with perturbative breaking of supersymmetry were studied in the case of minimal embedding of the standard model.[64] The main signature of the large extra dimension(s) in these constructions

is the appearance of a tower of excitations for the gauge bosons and Higgs bosons with the same gauge quantum numbers. Kaluza–Klein (KK) states are a straightforward consequence of all models with compactified dimensions, and they have masses

$$m_n^2=m_0^2+\frac{\mathbf{n}^2}{R^2}, \tag{243}$$

where R denotes the common radius of the D large internal dimensions, $\mathbf{n}$ is a D-dimensional vector, and m_0 denotes R-independent contributions coming from the electroweak symmetry breaking. All massive KK states are unstable, and they decay into quarks and leptons with a lifetime $O(10^{-26})$ sec when the size of the compact dimension(s) is $O(1)$ TeV^{-1}. The present experimental limits have been obtained from an analysis of the effective four-fermion operators which arise from exchange of the massive KK modes.[66] In orbifold models the current limits are $R^{-1}\geqslant 185$ GeV for one large extra dimension, and $R^{-1}\geqslant 1.4$ TeV, 1.1 TeV and 1 TeV for two large dimensions in the case of Z_3, Z_4, and Z_6 orbifolds, respectively.[66]

Among the KK excitations of different spins, the easiest to detect at LHC are the vectors with the quantum numbers of the electroweak $SU_L(2)\otimes U(1)$ gauge bosons. The most efficient way of observing KK states in proton–proton collisions is to identify charged leptons $l^{\pm}$ in the final state. The main background comes from the Drell–Yan process $pp\to l^+l^-+X$ with $l=e,\mu$. In many models with large compactified dimension(s) due to accidental suppression of the effective coupling constant of the massive $SU(2)$ vector excitations, only the $U(1)$ vector excitations couple to leptons. The masses of these states are given by Eq. (243), and they couple to fermions through the effective interaction

$$g'^*(p)\bar{\psi}^k\gamma_\mu(v_k+a_k\gamma_5)\psi^k B_n^{*\mu}, \tag{244}$$

where k labels the different species of fermions, and $g'^*(p)$ is an effective coupling constant at scale p. The interaction (244) leads to rates of N_n^* decays into fermions given by

$$\Gamma(B_n^*\to f\bar{f})=(g'^*(m_n))^2\frac{m_n}{12\pi}C_f(v_f^2+a_f^2), \tag{245}$$

while the corresponding interaction with their scalar superpartners $\tilde{f}_{R,L}$ leads to the decay rates

$$\Gamma(B_n^*\to\bar{\tilde{f}}_{R(L)}\tilde{f}_{R(L)})=(g'^*(m_n))^2\frac{m_n}{48\pi}C_f(v_f\pm a_f)^2, \tag{246}$$

where $C_f=1$ or 3 for color singlets or triplets, respectively. The total width is

$$\Gamma_n=\frac{5}{8\pi}(g'^*)^2 m_n. \tag{247}$$

The total cross section for production of the KK excitations B_n^* is given by[61]

$$\sigma_t=\sum_{\text{quarks}}\int_0^{\sqrt{s}}dM\int_{\ln M/\sqrt{s}}^{\ln\sqrt{s}/M}dy\,q_q(y,M)S_q(y,M), \tag{248}$$

where

$$g_q(y,M)=\frac{M}{18\pi}x_a x_b[f_q^{(p)}(x_a,M)f_{\bar{q}}^{(p)}(x_b,M)+f_{\bar{q}}^{(p)}\times(x_a,M)f^{(b)}(x_b,M)] \tag{249}$$

and

$$S_q(y,M)=(g'^*)^4\frac{1}{N}\sum_{|\vec{n}|<R\sqrt{s}}\frac{(v_q^2+a_q^2)(v_l^2+a_l^2)}{(M^2-m_n^2)^2+\Gamma_n^2 m_m^2}, \tag{250}$$

in which $x_a=(M/\sqrt{s})e^y$, $x_b=(M/\sqrt{s})e^{-y}$, and the factor N comes from Z_N orbifold projection. The main background comes from the Drell–Yan production mechanism. The main conclusion of Ref. 61 is that at LHC for $L_t=10^5$ pb^{-1} it would be possible to obtain a bound $R^{-1}\geqslant 4.5$ TeV on the compactification radius.

Compositeness. A composite structure for quarks would appear in the form of deviations from the standard QCD expectations at high transverse momenta, where valence-quark scattering dominates. It is expected that it would be possible to discover a quark compositeness scale with $\Lambda_c\leqslant 10$ TeV. The best way to look for lepton compositeness effects is to study lepton pair production at large dilepton invariant masses. It would be possible to discover lepton compositeness for $\Lambda_{\text{lept}}\leqslant 20$ TeV.[2]

Nonstandard Higgs bosons. Many Higgs-doublet models, in which each Higgs doublet couples to its own quark with a relatively large Yukawa coupling constant, were considered in Ref. 66. For appreciable Yukawa coupling constants the main reaction for production of the Higgs doublets corresponding to the first and second generations is quark–antiquark fusion. The phenomenology of the Higgs doublets corresponding to the third generation is very similar to the phenomenology of the model with two Higgs doublets. The cross section for quark–antiquark fusion in the quark–parton model in the approximation of infinitely narrow resonances is given by the standard formula

$$\sigma(AB\to HJ_{q_iq_j}+X)=\frac{4\pi^2\Gamma(H_{q_iq_j}\to\bar{q}_iq_j)}{9sM_H}\int_{M_H^2/s}^1\frac{dx}{x}\times[\bar{q}_{Ai}(x,\mu)q_{Bj}(x^{-1}M_H^2s^{-1},\mu)+q_{Aj}(x,\mu)\bar{q}_{Bj}(x^{-1}M_H^2s^{-1},\mu)]. \tag{251}$$

Here $\bar{q}_{Ai}(x,\mu)$ and $q_{Aj}(x,\mu)$ are the parton distributions of the antiquark $\bar{q}_i$ and quark q_j in hadron A at the normalization point $\mu\sim M_H$, and $\Gamma(H_{q_iq_j}\to\bar{q}_iq_j)$ is the hadronic width for decay of the Higgs boson into a quark–antiquark pair. For the Yukawa Lagrangian

$$L_Y=h_{q_iq_j}\bar{q}_{Li}q_{Rj}H_{q_iq_j}+\text{H.c.}, \tag{252}$$

the hadronic decay width for massless quarks is

$$\Gamma(H_{q_iq_j}\to\bar{q}_iq_j)=\frac{3M_Hh_{q_iq_j}^2}{16\pi}. \tag{253}$$

The value of the renormalization point μ was choosen to be the mass M_H of the corresponding Higgs boson. Variation of the renormalization point μ in the interval $0.5M_H$–$2M_H$ leads to variation of the cross section by less than 50%. In

the considered models there are Higgs bosons which couple to both down quarks and leptons, and so the best signature is the search for electrically neutral Higgs-boson decays into e^+e^- or $\mu^+\mu^-$ pairs. As regards charged Higgs bosons, the best way to detect them is to look for their decays into charged leptons and neutrinos. Higgs doublets which couple to up quarks in the model with massless neutrinos do not couple to leptons, and so the only way to detect them is to search for a resonance-type structure in the distribution of the dijet cross section in the dijet invariant mass, as in the case of all Higgs bosons, since in the considered models all Higgs bosons decay mainly into quark–antiquark pairs, leading at the hadron level to additional dijet events. However, the accuracy of the determination of the dijet cross section is $O(1)$ percent, so that it would not be so easy to find a stringent bound on the Higgs-boson mass by measurement of the dijet differential cross section at LHC. In the considered Higgs-doublet models, owing to the smallness of the vacuum expectation values of the Higgs doublets corresponding to the u, d, s, and c quarks, after electroweak symmetry breaking the mass splitting inside the Higgs doublets is small, so that in such models the search for a neutral Higgs boson decaying into a lepton pair is in fact the search for the corresponding Higgs isodoublet. The main background in the search for neutral Higgs bosons through their decays into lepton pairs is the Drell–Yan process, which is under control. The main conclusion of Ref. 66 is that at LHC for $L_t = 10^5$ pb^{-1} and for the corresponding Yukawa coupling constant $h_Y = 1$ it would be possible to detect such Higgs bosons with masses up to 4.5–5 TeV.

Search for vector-like fermions. Vector-like fermions are characterized by having their left- and right-handed components transforming in the same way under the gauge symmetry group. Therefore, their mass terms $\bar{\psi}_L\psi_R$ are not forbidden by any symmetry. As a result, their masses are unbounded, and they decouple when they are taken to infinity. The standard model does not need vector-like fermions, and models with additional vector-like fermions are not very popular at present. Vector-like fermions decay by exchange of the standard electroweak gauge and Higgs bosons $W^{\pm}$, Z, h, all three being comparable in size.[67] It is possible to add to the standard model extra vector-like fermions with the following quantum numbers:

(a) Down singlet D quark.
(b) Up singlet U quark.
(c) Up–down quark doublet (U,D).
(d) Singlet charged lepton E.
(e) Singlet neutral lepton N.
(f) Neutral charged-lepton doublet (N,E).

The production cross sections are similar to those of the standard fermions.

Vector-like quarks decay mainly via $Q \to Wq_i$, Zq_i, hq_i modes, while vector-like leptons decay mainly via $L \to Wl$, Zl, hl modes. For vector-like quarks the branching ratios obey the approximate rule $W/Z/h \approx 2/1/1$. The signatures from vector-like quark-pair production at LHC with their subsequent decays are: 6-jet events, 2-lepton+4-jet events, and 4-lepton plus 2-jet events. The signatures from the vector-like lepton-pair production with their subsequent decays are: 6-lepton events, 4-lepton plus 2-jet events, and 2-lepton plus 4-jet events.

4. CONCLUSIONS

The large hadron collider can test the structure of many theories at the TeV scale. LHC will be capable of discovering the Higgs boson and low-energy broken supersymmetry with squark and gluino masses up to 2–2.5 TeV. There is also a nonzero chance of finding something new (Z' bosons, W' bosons, leptoquarks,...) at LHC. At any rate, after LHC we will know the basic elements of the structure of matter in the TeV region.

We are indebted to our colleagues from the INR theoretical department for useful discussions. The research described in this publication was made possible in part by Award No. RP1-187 of the U.S. Civilian Research and Development Foundation for the Independent States of the Former Soviet Union (CRDF).

[1)]To be precise, we review the main physics to be investigated at CMS.

[1] CMS, Technical Proposal, CERN/LHCC/94-38 LHCCP1 (1994).
[2] ATLAS, Technical Proposal, CERN/LHCC/94-43 LHCCP2 (1994).
[3] S. M. Berman, J. D. Bjorken, and J. B. Kogut, Phys. Rev. D **4**, 3388 (1971).
[4] See, for example: R. P. Feynman, *Photon–Hadron Interactions* (Benjamin, Reading, Mass., 1972); E. Eichten, I. Hinchlife, K. Lane, and C. Quigg, Rev. Mod. Phys. **56**, 579 (1984); **58**, 1065 (1986).
[5] See, for example: Yu. L. Dokshitzer, V. A. Khoze, A. H. Mueller, and S. I. Troyan, *Basics of Perturbative QCD* (Editions Frontières, Gif-sur-Yvette, 1991); G. Altarelli, Phys. Rep. **81**, 1 (1982); A. Bassetto, M. Ciafaloni, and G. Marchesini, Phys. Rep. C **100**, 201 (1983).
[6] J. Botts *et al.*, Phys. Lett. B **304**, (1993); MSUHEP 93-18.
[7] T. Sjostrand, Comput. Phys. Commun. **39**, 38 (1986); T. Sjostrand and M. Begtsson, Comput. Phys. Commun. **53**, 367 (1987); T. Sjostrand, CERN-TH.7112/93.
[8] M. Gluck, E. Hoffmann, and E. Reya, Z. Phys. C **13**, 119 (1982).
[9] P. Higgs, Phys. Lett. **12**, 132 (1964); F. Englert and R. Brout; Phys. Rev. Lett. **13**, 321 (1964).
[10] See, for example, Ta-Pei Cheng and Ling-Fong Li, *Gauge Theory of Elementary Particle Physics* (Oxford University Press, Oxford, 1984); S. Pokorsky, *Gauge Field Theories* (Cambridge University Press, Cambridge, 1987); V. I. Borodulin, R. N. Rogalyov, and S. R. Slabospitsky, Compendium of Relations, IHEP Preprint 95-50.
[11] Particle Data Group, Phys. Rev. D **50**, 1173 (1994).
[12] A. Blondel, Precision Electroweak Physics at LEP, CERN-PPE/94–133 (1994).
[13] B. W. Lee, C. Quigg, and C. B. Thacker, Phys. Rev. Lett. **38**, 883 (1977); Phys. Rev. D **10**, 1145 (1974).
[14] N. Cabibbo, L. Maiani, G. Parisi, and R. Petronzio, Nucl. Phys. B **158**, 295 (1979); M. Lindner, Z. Phys. C **31**, 295 (1986).
[15] N. V. Krasnikov, Yad. Fiz. **28**, 549 (1978) [Sov. J. Nucl. Phys. **28**, 279 (1978); P. Q. Hung, Phys. Rev. Lett. **42**, 873 (1979); H. D. Politzer and S. Wolfram, Phys. Lett. B **82**, 242 (1979)]; A. A. Anselm, JETP Lett. **29**, 590 (1979); M. Lindner, M. Sher, and M. Zaglauer, Phys. Lett. B **228**, 139 (1989).
[16] N. V. Krasnikov, G. Kreyerhoff, and R. Rodenberg, Mod. Phys. Lett. A **9**, 3663 (1994).
[17] H. Georgi *et al.*, Phys. Rev. Lett. **40**, 692 (1978).
[18] See, for example: J. F. Gunion, H. E. Haber, G. Kane, and S. Dawson, *The Higgs Hunter's Guide* (Addison-Wesley, Redwood City, CA, 1990).
[19] See, for example: Physics at LEP, Vol. 1: Standard Physics, edited by G. Altarelli, R. Kleiss, and C. Verzegnassi, CERN Yellow Report 86-02 (1986).
[20] R. D. Peccei and H. R. Quinn, Phys. Rev. Lett. **38**, 1440 (1977); V. Baluni, Phys. Rev. D **19**, 2227 (1979); R. J. Crewther *et al.*, Phys. Lett. B **88**, 123 (1979); **91**, 487(E) (1990).
[21] See, for example: I. I. Bigi *et al.*, in *CP Violation*, edited by C. Jarlskog

(World Scientific, Singapore, 1989); A. J. Buras, Nucl. Instrum. Methods Phys. Res. A **308**, 1 (1995). M. Gronau, Nucl. Instrum. Methods Phys. Res. A **368**, 21 (1995). M. Neubert, Mod. Phys. A. **11**, 4173 (1996).
[22] L. Wolfenstein, Phys. Rev. Lett. **51**, 1945 (1983).
[23] See, for example: N. Neubert, Mod. Phys. A **11** 4173 (1996).
[24] L. L. Chau and W. Y. Keung, Phys. Rev. Lett. **53**, 1802 (1984); C. Jarlskog and R. Stora, Phys. Lett. B **208**, 268 (1988).
[25] M. A. Shifman, A. I. Vainstein, and V. I. Zakharov, Nucl. Phys. B **120**, 316 (1977).
[26] K. Krisebom *et al.* (LHC-B), Letter of intent, CERN/LHCC 95-5 (1995).
[27] T. Nakada, in *Proceedings of the 3rd German–Russian Workshop on Heavy Quark Physics* edited by M. A. Ivanov and V. E. Lybovitskij (Dubna, 1996).
[28] A. Ali, CKM Update: a Review, Workshop Beauty 94, Mt. St. Michel, France, 1994; Nucl. Instrum. Methods Phys. Res. A **351**, 1 (1994).
[29] D. Denegri *et al.*, Nucl. Instrum. Methods Phys. Res. A **351**, 95 (1994).
[30] A. Ali, C. Creub, and T. Mannel, "Rare B decays in the standard model, DESY 93-016 (1993).
[31] See, for instance: H. C. Eggers and J. Rafelski, Mod. Phys. A **6**, 1067 (1991); C. P. Singh, Mod. Phys. A **7**, 7185 (1992); M. Jacob, Mod. Phys. A **11**, 4943 (1996).
[32] T. Matsui and H. Satz, Phys. Lett. B **178**, 416 (1986).
[33] NA50, LAPP/Annecy–Bucharest, IAP-Cagliari, CERN-LPC/Clermont–Ferrand–Cracow IPN, LIP/Lisbon–Moscow, INR-Orsay, IPN Orsay, LPNHE-Ecole Poly./Palaiseau–Strasbourg CNR, Torino–Lyon IPN Collaboration.
[34] G. Gershell and J. Hufner, Phys. Lett. B **207**, 257 (1988); J. Ftanik, P. Lichard, and J. Pisut, Phys. Lett. B **207**, 194 (1988); S. Gavin, M. Gyulassy, and A. Jackson, Phys. Lett. B **207**, 257 (1988).
[35] ALICE, Technical Proposal, CERN/LHCC/95-71 (1995).
[36] R. Kvatadze and R. Shanidze, "Jet recognition in heavy-ion collisions with CMS," CERN CMS TN/94-270 (1994).
[37] Reviews and original references can be found in: R. Barbieri, Riv. Nuovo Cimento **11**, 1 (1988); A. B. Lahanus and D. V. Nanopoulos, Phys. Rep. **145**, 1 (1987); H. E. Haber and G. L. Lane, Phys. Rep. **117**, 75 (1985); H. P. Nilles, Phys. Rep. **110**, 1 (1984).
[38] S. Ferrara, D. Z. Freedman, and P. Van Nieuwenhuizen, Phys. Rev. D **13**, 3214 (1976); S. Deser and B. Zumino, Phys. Lett. B **62**, 335 (1976); P. Van Nieuwenhuizen, Phys. Rep. **68**, 189 (1981); J. Wess and J. Bagger, *Supersymmetry and Supergravity* (Princeton University Press, Princeton, NJ, 1983).
[39] See, for example: M. B. Green, J. H. Schwarz, and E. Witten, *Superstring Theory*, (Cambridge University Press, Cambridge, 1987).
[40] See, for example: H. Dreiner and G. G. Ross, Nucl. Phys. B **365**, 597 (1991).
[41] N. Polonsky and A. Pomarol, Phys. Rev. Lett. **73**, 2292 (1994).
[42] N. V. Krasnikov and V. V. Popov, "PLANCKSUSY—new program for SUSY mass calculations: from Planck scale to our reality," INR Preprint 976TH/96.
[43] L. E. Ibanez and C. Lopez, Phys. Lett. B **126**, 54 (1983); Nucl. Phys. B **233**, 511 (1984); **256**, 218 (1985).
[44] See Ref. 37.
[45] W. de Boer, R. Ehret, and D. I. Kazakov, Z. Phys. C **67**, 647 (1995).
[46] J. Ellis, G. Ridolfi, and F. Zwirner, Phys. Lett. B **257**, 83 (1991); H. Haber and R. Hempfling, Phys. Rev. Lett. **66**, 1815 (1991); A. Yamada, Phys. Lett. B **263**, 233 (1991); R. Barbieri, M. Frigeni, and F. Caravaglis, Phys. Lett. B **258**, 233 (1991); P. M. Chanowski, S. Pokorski, and J. Rosick, Phys. Lett. B **275**, 191 (1992).
[47] N. V. Krasnikov and S. Pokorski, Phys. Lett. B **288**, 184 (1992).
[48] H. Baer *et al.*, "Low-energy supersymmetry phenomenology," CERN-PPE/95-45.
[49] H. Baer *et al.*, Phys. Lett. B **161**, 175 (1985); G. Gamberini, Z. Phys. C **30**, 605 (1986); H. Baer *et al.*, Phys. Rev. D **36**, 96 (1987); G. Gamberini *et al.*, Phys. Lett. B **203**, 453 (1988); R. M. Barnett, J. Gunion, and H. Haber, Phys. Rev. D **37**, 1892 (1988); A. Bartl *et al.*, Z. Phys. C **52**, 477 (1991).
[50] See, for example: H. Baer *et al.*, Mod. Phys. A **4**, 4111 (1989).
[51] Z. Kunszt and F. Zwirner, Nucl. Phys. B **385**, 3 (1992).
[52] S. Abddullin, SUSY Studies in CMS, LHCC/SUSY Workshop, CERN (1996).
[53] I. Iashvili, SUSY Studies in CMS, LHCC/SUSY Workshop, CERN (1996).
[54] D. Denegri, L. Rurua, and N. Stepanov, "Detection of sleptons and instrumental requirements in CMS," CMS Technical Note TN/96-059 (1996).
[55] N. V. Krasnikov, Mod. Phys. Lett. A **9**, 791 (1994); N. V. Krasnikov, Phys. Lett. B **388**, 783 (1996); N. Arkani-Hamed *et al.*, Phys. Rev. Lett. **77**, 1937 (1996).
[56] N. V. Krasnikov, Pis'ma Zh. Éksp. Teor. Fiz. **65**, 139 (1997) [JETP Lett. **65**, 148 (1997)].
[57] S. Dimopoulos *et al.*, Phys. Rev. D **41**, 2099 (1990); S. Dawson, Nucl. Phys. B **261**, 297 (1985); P. Binetruy and J. Gunion, INFN Eloisatron Project Working Group, 6th Workshop on Novel Features of High-Energy Hadronic Collisions, Erice, 1988; H. Dreiner and G. G. Rodd, Nucl. Phys. B **365**, 597 (1991).
[58] N. V. Krasnikov, Phys. Lett. B **386**, 161 (1996).
[59] N. V. Krasnikov, Phys. Lett. B **306**, 283 (1993); N. V. Krasnikov, G. Kreyerhoff, and R. Rodenberg, Nuovo Cimento A **107**, 589 (1994).
[60] N. V. Krasnikov, Preprint ENSLAPP-A-529-95; Pis'ma Zh. Éksp. Teor. Fiz. **61**, 236 (1995) [JETP Lett. **61**, 245 (1995)].
[61] I. Antoniadis, K. Benakli, and M. Quiros, Phys. Lett. B **331**, 313 (1994).
[62] T. Banks and L. Dixon, Nucl. Phys. B **307**, 93 (1988); I. Antoniadis, C. Bachas, D. Lewellen, and T. Tomaros, Phys. Lett. B **207**, 441 (1988).
[63] I. Antoniadis, Phys. Lett. B **246**, 377 (1990).
[64] I. Antoniadis, C. Munoz, and M. Quiros, Nucl. Phys. B **397**, 515 (1993).
[65] I. Antoniadis and K. Benakli, Preprint CPTH-A 0793 (1993).
[66] N. V. Krasnikov, Mod. Phys. Lett. A **10**, 2675 (1995).
[67] See, for example: F. del Agulia, Ll. Ametller, G. L. Kane, and J. Vidal, Nucl. Phys. B **334**, 1 (1990).

This article was published in English in the original Russian journal. It is reproduced here with the stylistic changes by the Translation Editor.